JGR Earth Surface

RESEARCH ARTICLE
10.1029/2021JF006339

Bedforms of Thwaites Glacier, West Antarctica: Character and Origin

R. B. Alley[1], N. Holschuh[2,3], D. R. MacAyeal[4], B. R. Parizek[1], L. Zoet[5], K. Riverman[6,7], A. Muto[8], K. Christianson[2], E. Clyne[1], S. Anandakrishnan[1], N. Stevens[5], and GHOST Collaboration[9]

[1]Department of Geosciences, and Earth and Environmental Systems Institute, Pennsylvania State University, University Park, PA, USA, [2]Department of Earth and Space Sciences, University of Washington, Seattle, WA, USA, [3]Department of Geology, Amherst College, Amherst, MA, USA, [4]Department of Geophysical Sciences, University of Chicago, Chicago, IL, USA, [5]Department of Geoscience, University of Wisconsin, Madison, WI, USA, [6]College of Earth, Ocean, and Atmospheric Sciences, Oregon State University, Corvallis, OR, USA, [7]Department of Environmental Studies, University of Portland, Portland, OR, USA, [8]Department of Earth and Environmental Science, Temple University, Philadelphia, PA, USA, [9]The list of authors is provided in Appendix A (https://thwaitesglacier.org/projects/ghost)

Abstract Bedforms of Thwaites Glacier, West Antarctica both record and affect ice flow, as shown by geophysical data and simple models. Thwaites Glacier flows across the tectonic fabric of the West Antarctic rift system with its bedrock highs and sedimentary basins. Swath radar and seismic surveys of the glacier bed have revealed soft-sediment flutes 100 m or more high extending 15 km or more across basins downglacier from bedrock highs. Flutes end at prominent hard-bedded moats on stoss sides of the next topographic highs. We use simple models to show that ice flow against topography increases pressure between ice and till upglacier along the bed over a distance that scales with the topography. In this basal zone of high pressure, ice-contact water would be excluded, thus increasing basal drag by increasing ice-till coupling and till flux, removing till to allow bedrock erosion that creates moats. Till carried across highlands would then be deposited in lee-side positions forming bedforms that prograde downglacier over time, and that remain soft on top through feedbacks that match till-deformational fluxes from well upglacier of the topography. The bedforms of the part of Thwaites surveyed here are prominent because ice flow has persisted over a long time on this geological setting, not because ice flow is anomalous. Bedform development likely has caused evolution of ice flow over time as till and lubricating water were redistributed, moats were eroded and bedforms grew.

Plain Language Summary Thwaites Glacier, West Antarctica, is of great interest because ongoing retreat could lead to faster future changes that could notably increase sea-level rise. Wide-ranging studies are thus focused on gaining broad understanding of the glacier. Geophysical surveys discussed here show that the bed of the glacier has been sculpted by the flowing ice, eroding large "moats" upglacier and to the sides of bedrock obstacles, and depositing long tails of soft sediment downglacier of those obstacles. We use simple models to show that these features formed over time because of the interactions among ice, bedrock, and subglacial water and sediment, and that the behavior of the glacier must have changed as these features developed. This knowledge does not directly affect estimates of the potential for future sea-level rise, but does guide further studies to improve those estimates. This knowledge also may help understand the formation of glacially sculpted landscapes left in widespread regions by former ice sheets.

1. Introduction

Subglacial bedforms, such as drumlins and mega-scale glacial lineations (MSGLs), have long intrigued Earth scientists. An annotated bibliography on drumlins published in the year 1984, for example, included 1,027 references (Menzies, 1984), and the literature has grown substantially since then.

Bedforms both influence and record the flow of ice and sediment (e.g., Spagnolo et al., 2014). Voluminous literature indicates that interest remains high in part because of a widespread belief that these influences and records are not yet fully understood, and that additional useful information about subglacial processes should be available from better interpretation of these features.

The members of the Geophysical Habitat of Subglacial Thwaites (GHOST) Collaboration team are provided in Appendix A (https://thwaitesglacier.org/projects/ghost).

Key Points:

- Extensive, well-developed bedforms occur beneath upglacier regions of Thwaites Glacier, West Antarctica where ice flow is unremarkable
- Pressure variations from ice flow over bedrock topography caused erosion and deposition, producing stoss-side moats and lee-side flutes
- Bedforms both record and influence ice flow

Supporting Information:

Supporting Information may be found in the online version of this article.

Correspondence to:

R. B. Alley,
rba6@psu.edu

Citation:

Alley, R. B., Holschuh, N., MacAyeal, D. R., Parizek, B. R., Zoet, L., Riverman, K., et al. (2021). Bedforms of Thwaites Glacier, West Antarctica: Character and origin. *Journal of Geophysical Research: Earth Surface*, *126*, e2021JF006339. https://doi.org/10.1029/2021JF006339

Received 29 JUN 2021
Accepted 11 OCT 2021

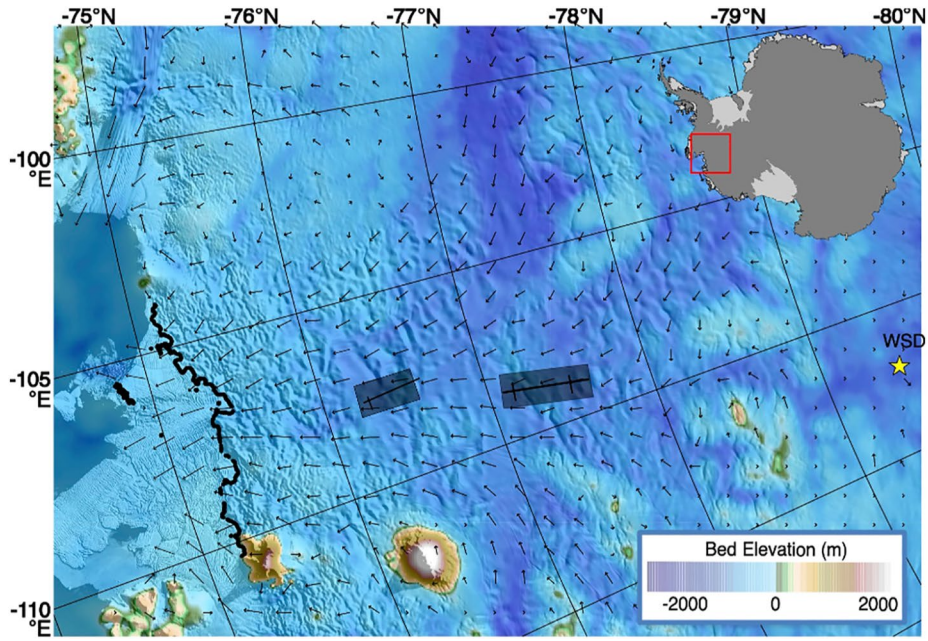

Figure 1. Location map, with inset showing location in Antarctica. Radar surveys were conducted in the shaded boxes, and seismic data were collected along the black lines in those boxes. Figure is modified from Clyne et al. (2020), with ice-flow velocities (arrows; NASA MEaSUREs InSAR-derived data from Rignot et al., 2017), bed elevation from Bedmap2 (Fretwell et al., 2013), and the grounding line in 2011 (black line) based on NASA InSAR (Rignot et al., 2016; following; Muto, Anandakrishnan, et al., 2019). The yellow star shows the West Antarctic Ice Sheet Divide ice coring site.

Difficulty interpreting bedforms likely arises at least in part from their complicated history. The most-studied features are generally on deglaciated land surfaces, which have experienced one or more cycles of ice advance and retreat, so that the bedforms reflect the integrated effects of complex ice-marginal processes perhaps further overprinted by post-glacial processes. These ice-marginal processes may be essential for formation of the bedforms, but may also obscure the essential processes that occurred farther from the ice margin, or both. Subglacial conditions farther from the margin of the ice sheet are recorded more clearly in deposits of those marine-ending glaciers that experienced relatively rapid "lift off" during retreat, together with relatively small grounding-zone and postglacial sedimentation rates, preserving the "death mask" of the ice sheet without modification during retreat (e.g., Davies et al., 2017; Spagnolo et al., 2014; Wellner et al., 2006); however, this provides a somewhat restricted sample of glaciers.

Geophysical surveys of modern glaciers have long been used to characterize their beds (e.g., Drewry et al., 1983), including assessments of roughness and resolvable bedforms. These surveys are largely inadequate for many bedform studies, however. The Antarctic has roughly 0.1 km of radar flightline for each 1 km^2 of area, for example (Morlighem et al., 2020), surely not enough to identify and characterize most bedforms (compare to ~0.7 km of road for each km^2 of area in the USA including Alaska, or ~1.7 km/km^2 in the UK with even larger ratios in much of the EU; OECD, 2015). Very dense grids of geophysical lines have occasionally been collected that do allow characterization of bedforms (e.g., Bingham et al., 2017; King et al., 2009; Smith et al., 2007), but such data collection is logistically difficult, so very few areas have been characterized in this way.

As reported by Holschuh et al. (2020), however, swath radar now can produce high-resolution three-dimensional maps covering larger areas of modern glacier beds, with sufficient detail to allow meaningful comparisons to terrestrial LiDAR and marine side-scan sonar. Results of the survey reported by Holschuh et al. (2020) over two upstream portions of Thwaites Glacier (Figure 1), part of the West Antarctic Ice Sheet (WAIS), are shown in Figure 2. After a short review of the Thwaites setting, we discuss many of the features shown in Figure 2, and develop hypotheses for their formation. We provide simple models in support of the hypotheses, and briefly discuss some of the problems in conducting comprehensive modeling, but do not attempt this much-more-difficult task. We hypothesize that: the high-pressure zones generated by flow against stoss sides of bedrock obstacles exclude much of the ice-contact basal water; this couples ice more strongly to till to increase till deformational

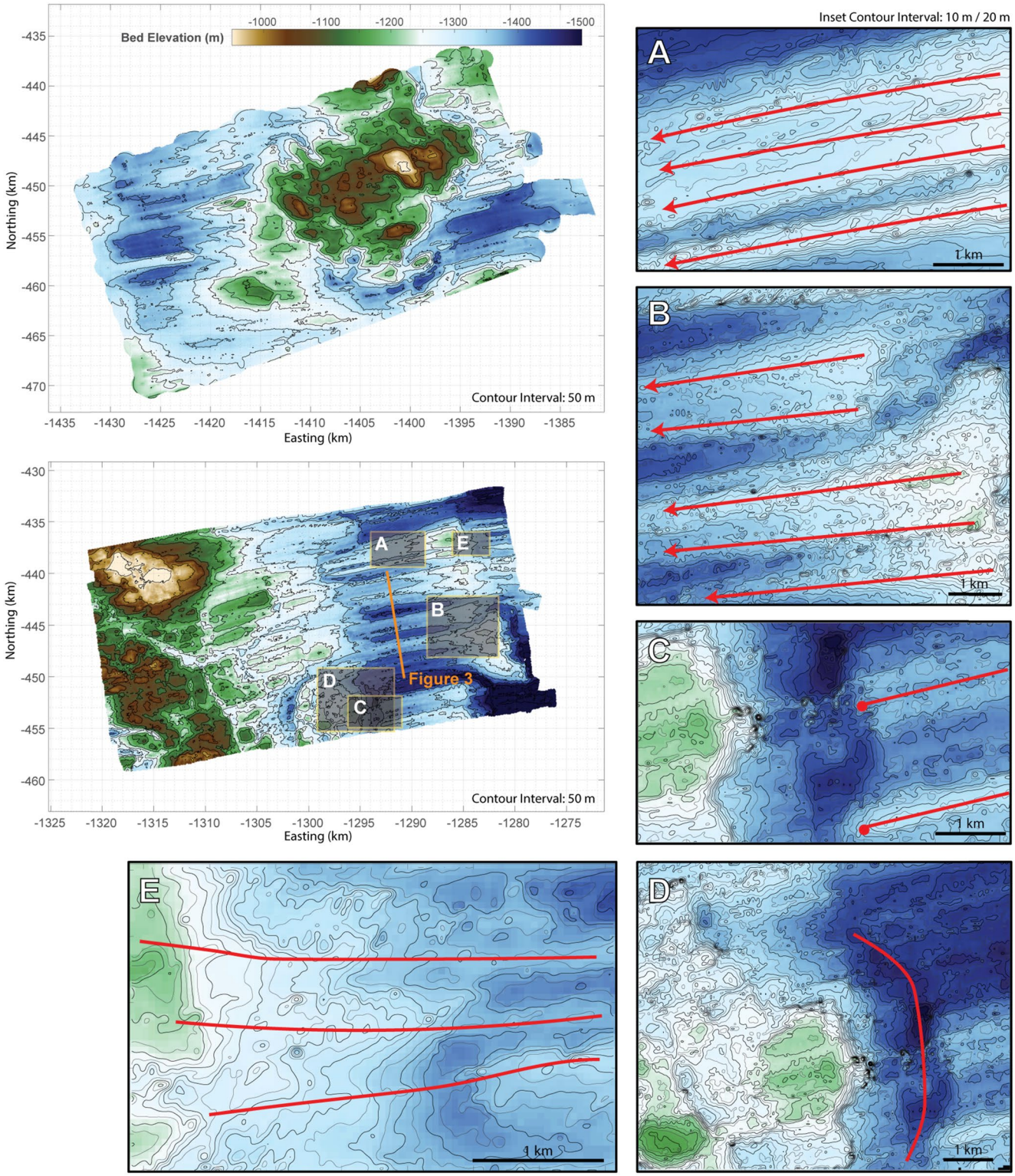

Figure 2. Swath-radar-derived topographic maps of the glacier bed, from Holschuh et al. (2020), for the downglacier (upper left panel) and upglacier (center left panel) survey blocks indicated in Figure 1, together with annotated subregions of the upglacier block (A–E), as discussed further below. Smallest grid spacings are 1 km. Color scale is in common for all panels, with deepest blue 1,500 m below sea level, and light tan 950 m below sea level, as indicated at upper left. Contour interval is 50 m.

flux; the resulting till divergence exposes bedrock to erosion; the erosion produces moats; the moats then influence subglacial water flow and lubrication; furthermore, till transported across bedrock obstacles is deposited in low-pressure lee-side positions to form prograding, soft-topped flutes; and, water diversion to the low-pressure lee-side areas favors erosion and greater basal drag in troughs. After developing this hypothesis, we provide a cartoon of it as Figure 7.

2. Motivation—Thwaites Glacier Bedforms

2.1. Geological Setting and Glacier Dynamics

Thwaites Glacier is arguably the most important ice-flow feature for near-future sea-level rise (e.g., Scambos et al., 2017). Models have repeatedly shown that Thwaites is vulnerable to retreat, which beyond some threshold could become both rapid and difficult to reverse, with the potential to raise global average sea level by more than 3 m over the following decades to centuries through retreat extending into neighboring drainages (e.g., DeConto & Pollard, 2016; Joughin et al., 2014; Parizek et al., 2013).

The marine basins of WAIS, where rapid deglaciation is most likely to occur, occupy extended, down-dropped crust of the West Antarctic Rift System (WARS) (e.g., Behrendt, 1999; Bingham et al., 2012; Winberry & Anandakrishnan, 2004). The Transantarctic Mountains form one well-defined rift flank, with Marie Byrd Land and other highlands along the Pacific (Amundsen Sea) coast forming the other rift flank. A tectonic fabric, controlled at least in part by extensional faults (e.g., Behrendt, 1999; Muto et al., 2013), runs parallel to those boundaries. Much of the ice flow is directed along this tectonic fabric, especially toward the Ross Embayment along the ice streams of the Siple Coast. But, because this rift basin forms an elongated channel with an extended flow path from its central region to the outlets, ice has built up sufficiently over that central part of WARS to drive flow across the tectonic fabric through gaps in the Pacific rift flank, especially at Thwaites Glacier.

Ice flow typically is directed down the ice-air surface slope (e.g., Cuffey & Paterson, 2010) and routinely crosses basal topography; however, most major ice streams still flow primarily parallel to basal topography (e.g., Bentley, 1987; Morlighem et al., 2020). Thwaites is extreme in having so much flow across such strongly transverse topography. This cross-topography flow may favor generation of bedforms.

Available data indicate that the bedforms of Thwaites Glacier have been formed over long times involving flow processes that still are active today. Paleoclimatic data indicate that the interior regions of WAIS have been continuously present with roughly their modern volume for at least ~100,000 years and possibly much longer, and have been present for most of the last few million years (reviewed by R. B. Alley et al., 2015, pp. 209–212). Retreat behind the modern grounding zone did occur during the mid-Holocene in the thin ice over the nearly horizontal bed of the Siple Coast (Kingslake et al., 2018) and perhaps elsewhere, but with no evidence of recent major retreat into the deep interior basins (e.g., Johnson et al., 2017).

Punctuated rapid subglacial lake drainage could be responsible for bedform formation at Thwaites, but we consider this possibility unlikely. Subglacial lake drainages occur locally in the modern environment (Hoffman et al., 2020; Malczyk et al., 2020; Smith et al., 2017), but the water-flow rates thus far observed from subglacial Antarctic lakes do not appear to be fast enough to be geomorphically important (also see R. B. Alley, Cuffey, & Zoet, 2019, p. 3). Furthermore, the features such as stoss-side moats and lee-side tails that we describe below are widespread, and not focused in modern water-flow pathways as generally calculated assuming that subglacial hydrologic potential arises from elevation and the overburden pressure of the ice (e.g., Holschuh et al., 2020). We remain interested in the possibility that much larger floods have occurred, perhaps during WAIS growth or regrowth, discharging water trapped by grounding of ice shelves bridging the deep basins (R. B. Alley et al., 2006; also see Kirkham et al., 2019), but any such floods linked to ice-sheet regrowth must be at least tens of thousands of years in the past. We thus assume that the bed of Thwaites Glacier in our inland study area has developed in response to long-term ice flow more-or-less like today for at least tens of thousands of years (e.g., Cuffey et al., 2016; Pollard & DeConto, 2009; Whillans, 1976), and thus that analyses starting from a steady-state assumption may be useful, something that may not be true for most or all bedforms that have been well-studied in deglaciated regions.

The geological setting of Thwaites exerts a first-order control on ice-sheet retreat behavior, and thus has helped guide research priorities. At present, the grounding zone is somewhat stabilized on a transverse bedrock sill in

the rift flank (e.g., Sergienko & Hindmarsh, 2013), and the most important question going forward is probably whether the grounding zone will retreat from this sill. In some locations, particularly on the eastern tributary, the grounding line has already started to retreat from this sill (Millilo et al., 2019). If further retreat occurs, numerical models tend to simulate continuing retreat, often quite rapidly, although with slowdowns on deeper transverse ridges farther upglacier; this focuses attention on 3-d bathymetry, with strong dependence on the loss or persistence and strength of ice-shelf buttressing, and on estuarine processes in the grounding zone (e.g., K. E. Alley, Scambos, et al., 2019; R. B. Alley, Cuffey, & Zoet, 2019; Horgan et al., 2013; Joughin et al., 2014; Morlighem et al., 2020; Parizek et al., 2013; Sun et al., 2020).

But, models also show that retreat behavior depends on processes controlling motion at the ice-bed interface as well as on bathymetry. As discussed below, the form of the basal "flow law" or friction law for ice motion is probably different between the stoss and lee sides of the subglacial ridges (e.g., Muto, Anandakrishnan, et al., 2019; Muto, Alley, et al., 2019), with more-nearly viscous behavior on stoss sides where bedrock is exposed, and more-nearly plastic behavior on lee sides where deformation of tills lubricates flow (Zoet & Iverson, 2020). Modeling suggests that a more-nearly plastic bed initially delays grounding-zone retreat in response to oceanic forcing, but accelerates retreat once initiated (Parizek et al., 2013). Modeling also suggests that, under some conditions, ice-flow behavior over a bed with alternating till and bedrock will fall between behaviors with the end-member beds, but under other conditions the alternating bed may exhibit novel behavior falling outside the end-members (Koellner et al., 2019). Thus, we focus here on the interactions between ice and rock that both govern future behavior and act to reshape the subglacial landscape.

We start by highlighting certain features on the bed of Thwaites Glacier, as recently published from swath radar and ground seismic surveys, that we consider to be especially important in providing clues to the controlling processes. We then construct simplified models of flow over such features, documenting large perturbations on the local pressure field. We synthesize these to hypothesize that effects of these pressure perturbations modify subglacial processes in ways that initiate and stabilize the observed subglacial bedforms.

2.2. Bed Morphology and Swath Radar

We focus on selected areas in the swath radar data shown in Figure 2. We refer to hard (consolidated, likely lithified sedimentary rock) and soft (till) beds, based on co-located seismic observations that have been published in several papers, as discussed in the following section.

The data in Figure 2 show that:

1. Streamlining of the bed is widespread to ubiquitous (features are elongated along ice flow, with greater variability in bed elevation across flow than along flow);
2. Elongated bedforms composed of soft till locally exceed 100 m in height and more than 15 km in length (and arguably much more; see below);
3. At least some of the broader bedforms (extending a few kilometers transverse to flow) are surmounted by narrower features that parallel each other and that parallel the larger features (Figures 2a and 2b); still-smaller features, if they exist, would have been difficult to resolve with the available data;
4. The most prominent elongated features (which might be called flutes, or MSGLs) occur in the down-dropped sedimentary basins with their "soft" tills, but these features are tails of crag-and-tail features starting in the lee of bedrock knobs in the "hard" uplands (Figure 2b);
5. Bedforms typically continue downglacier with little change in size until they approach the next major geologic boundary (the edge of the next fault block or bedrock-controlled high) (Figure 2c). Bedrock knobs are more common in the highlands, so the distance to the next bedrock-controlled high is shorter there, perhaps explaining at least in part why the bedforms are shorter there;
6. The downglacier transitions from soft till to bedrock knobs, where flutes end or at least become greatly reduced in size, are often marked by moats (sometimes called sichelwannen; see Holschuh et al., 2020). These are overdeepened regions upglacier of and extending to the sides of the bumps. The bed elevation typically drops by more than 10 m into the moats, and in some places by more than 50 m (Figure 2d). Moats are generally deepest directly upglacier of an obstacle but are typically traceable around the sides into lows between lee-side flutes (we will return later to the possibility that smaller moats also exist on the downglacier sides of bumps);

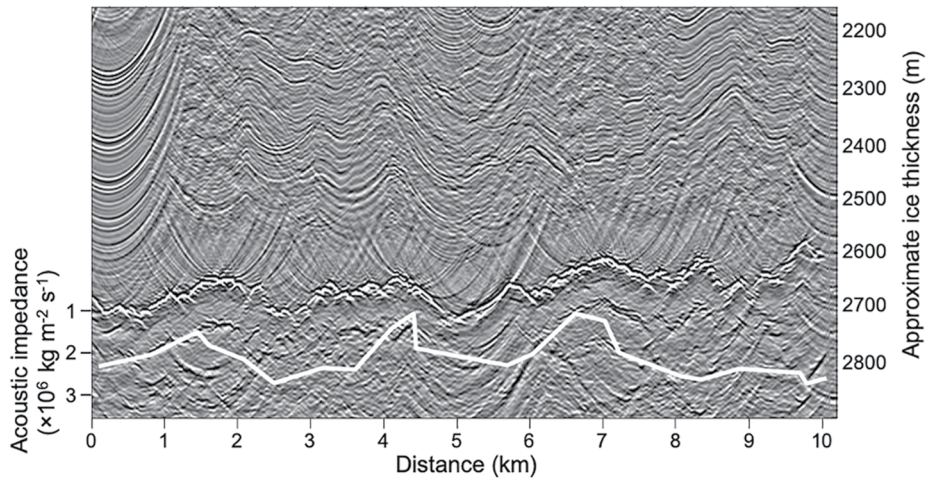

Figure 3. Bed of Thwaites Glacier along the upglacier cross-line in the upglacier grid shown in Figure 1, from Muto, Anandakrishnan, et al. (2019, their Figure 3 V line, which also plots the generally small uncertainties), looking downglacier. The stacked and migrated seismic section shows the prominent reflection from the bed between 2,600 and 2,700 m ice thickness (right-hand scale). The topographic highs are lee-side bedforms of bedrock features upglacier. Acoustic-impedance data are shown by the white line, which connects the individual measured data points. Note that the scale is inverted, so that "softer" beds plot upwards. All observed values on this profile indicate a relatively soft bed or perhaps water. The relation between topography and acoustic impedance is not entirely consistent, but tends to indicate that the bedform crests are softer than the troughs.

7. Careful examination shows many cases in which a flute appears to cross a moat and continue across highland topography, although with much-reduced amplitude of the flute. The available data are probably insufficient to insist that these are dynamically continuous, but they appear to be (Figure 2e). If they are continuous, then some bedforms are much longer than 15 km.

2.3. Bed Properties From Active-Source Seismic Surveys

Active-source seismic surveys were conducted during in the 2008–2009 and 2009–2010 austral summers along the survey lines shown in Figure 1. Collection, processing, data availability, and the main results are presented by Muto, Anandakrishnan, et al. (2019); Muto, Alley, et al. (2019); and Clyne et al. (2020).

Of greatest relevance here, the seismic data show, as discussed in those papers and in Figure 3:

1. Quite low acoustic impedance, indicating soft, water-saturated, dilated and deforming till, in lee-side positions including the major basins, as well as in smaller regions downglacier of bedrock bumps, and occasionally with seismically detectable free water;
2. Somewhat higher acoustic impedance, consistent with weakly lithified sedimentary rocks (and, very locally in the downglacier grid, crystalline rocks), on stoss sides of major topographic features, and, although with fewer samples, in deeper parts of moats;
3. Low acoustic impedance on crests of the bedforms where crossed by seismic lines, with data likely showing that the crests are even softer than the troughs, and no evidence of consistently harder crests than troughs (Figure 3).

The seismic surveys do not consistently image reflectors within the bed, but it is likely that strong, shallow and sharp material contrasts within the bedforms would have been identified if they existed. As noted by Muto, Anandakrishnan, et al. (2019), the ¼-wavelength vertical resolution in ice is ~6.4 m, and roughly half that much in soft till, based on peak frequency of ~150 Hz in the primary reflections, with Fresnel-zone width of ~365 m at the average depth of ~2,600 m in the upglacier grid, so laterally extensive beds more than ~3–4 m thick in the soft sediment could be resolved (e.g., Christianson et al., 2014). Interpretations are complicated by off-axis reflections from adjacent bedform crests that might obscure other returns, and by the relatively small seismic shot

sizes used, which were optimized for studying the ice-bed interface rather than deeper features. Pending additional data, it appears that the bedforms are somewhat homogeneous at least in their upper parts.

We thus seek to provide insight to the formation of these widespread, highly elongated, soft-topped, relatively homogeneous bedforms that occur at multiple scales up to and including >15 km long and >100 m high beneath Thwaites Glacier, which generally start in the lee sides of structurally controlled bedrock highs, and end, or at least are reduced in size, at stoss-side moats of the next structurally controlled bedrock features. The development of bedforms must both reflect and cause heterogeneity in the stress field at the base of Thwaites glacier. Next, we investigate the effects of the bedrock flow obstructions on the subglacial pressure field, with implications for local erosion, deposition, and water routing. We use diagnostic models that provide intuition for bedform evolution, building on prior ideas such as those in Muto, Anandakrishnan, et al. (2019), Muto, Alley, et al. (2019) and Holschuh et al. (2020), but originating much earlier, as described next.

3. Theory and Modeling—Influence of Bedforms on the Local Pressure Field

Fluctuations in bed-normal stress arising from ice flow over basal topography have long been central to models of basal processes (the review by Cuffey & Paterson, 2010 in Chapters 6 and 7 is a useful starting point). In flow past an obstacle, the pressure is raised on the upstream side and lowered on the downstream side to drive the flow divergence and convergence needed to negotiate the obstacle. We consider obstacles on horizontal beds, rather than sine-wave beds or other possible geometric models, to approximate the observed conditions of Thwaites with fault-controlled highlands upglacier of nearly planar, nearly horizontal lowlands.

We recognize the large uncertainties in basal conditions (no-slip to free-slip, till deformation following a "law" that may range between viscous and perfectly plastic, ice deformation exhibiting a power-law dependence on stress that may range from squared to fourth power or even a wider range); thus, no single model can be taken to represent behavior accurately. We thus emphasize those features that are found in common across a wide range of models that likely span the natural conditions, and we use these common features in developing hypotheses for bedform development. We start with the classical Stokes solution for a falling sphere, then consider Weertman (1957) sliding over a "tombstone," and follow with numerical models exploring a range of boundary conditions.

3.1. Idealized Models

Stokes (1851), in considering the motion of a pendulum, developed an analytic solution for flow of a viscous fluid past a sphere. This situation has many physical similarities to flow of linear-viscous ice over a well-lubricated horizontal bed across a no-slip hemispherical obstacle. In this classical Stokes (1851) model, flow of a fluid of viscosity μ past a spherical body of radius R moving at velocity U, the pressure P differs from the unperturbed value $P\infty$ at great distance, with dependence on distance r from the center of the sphere according to:

$$P - P\infty = 3\mu UR\cos\theta \,/\, \left(2r^2\right) \tag{1}$$

where θ is the polar angle from the far-field velocity vector.

Integrating this pressure perturbation over the surface of the sphere gives the contribution to the Stokes drag; 1/3 arises from pressure forces and 2/3 from viscous forces (e.g., Childress, 2009, Equations 7.34 and 7.38, from Stokes, 1851, Section II.18). The pressure perturbation is largest on the surface of the sphere, at $r = R$, and decreases into the fluid with an e-folding length of R*e^{½}, thus scaling with the sphere size. The pressure perturbation is largest along the diameter of the sphere parallel to the far-field flow, with elevated pressure on the stoss side and reduced pressure in the lee. Note that the pressure perturbation continues to the side of the sphere, falling to zero only along the circumference oriented perpendicular to the far-field flow ($\theta = 90°$) (aspects of this solution are shown in Figure 6, below).

Instead of the Stokes model, glaciologists have often found it more appropriate to start with the Weertman (1957) solution for basal sliding over a cubic "tombstone" obstacle of side length L on an otherwise frictionless, planar horizontal bed with free slip along the surfaces of the obstacle. In this model, far from the obstacle the stresses are $\sigma_x = \sigma_y = \sigma_z$, with x oriented horizontally along the far-field flow, and the pressure is

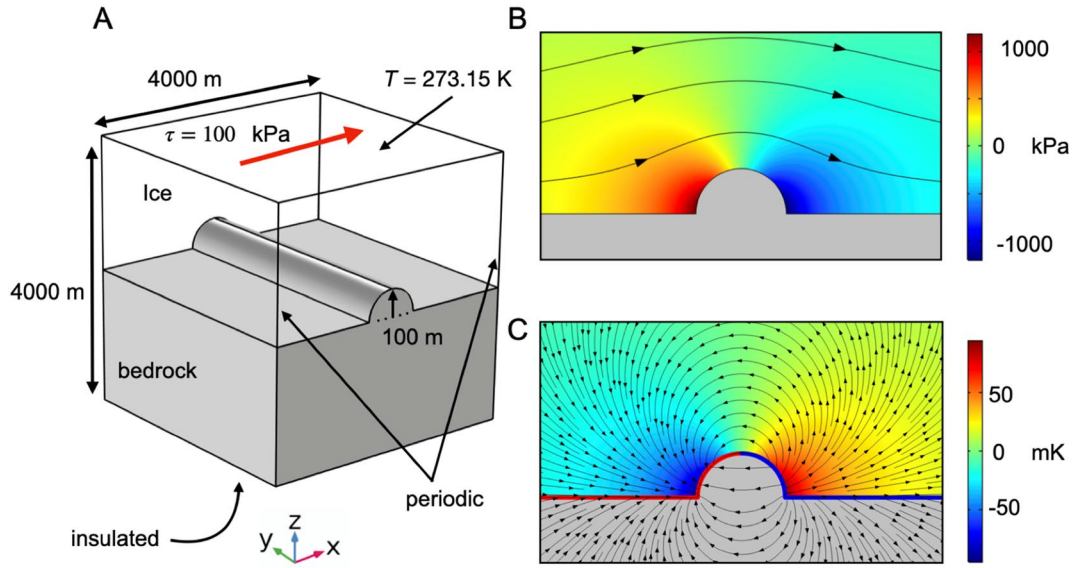

Figure 4. COMSOL model for flow of viscous ice (with viscosity of 10^{13} Pa s) over a bedrock obstacle. (a) Geometry used. This is a 2-d (vertical and along-flow) simulation, shown extended in the third (transverse) dimension here. (b) Ice-flow vectors, together with pressure field shown as perturbations with scale bar on right. (c) Heat flow vectors in ice and bed, together with temperature field in ice shown as perturbations with scale bar on right. The ice-rock interface is shown red where there is net heat flow convergence, supporting melting, and blue where there is net heat flow divergence, supporting freeze-on.

$$P\infty = \left(\sigma_x + \sigma_y + \sigma_z\right) / 3 = 3\sigma_x / 3 = \sigma_x \tag{2}$$

In the Weertman approximation, the x-directed stress is increased by $d\sigma_x$ in a volume of ice extending over a distance L upglacier of the obstacle over the area of the obstacle. In that region of perturbed stress, the pressure can be estimated as

$$P = \left(\sigma_x + d\sigma_x + \sigma_y + \sigma_z\right) / 3 = P\infty + d\sigma_x / 3 \tag{3}$$

$$P - P\infty = d\sigma_x / 3 \tag{4}$$

Hence, the pressure is increased by 1/3 of the added longitudinal stress. MacAyeal (2019) used COMSOL Multiphysics® finite element modeling to show (e.g., in his Figure 4), that the situation cannot be quite this simple, and that the high-pressure region extends upglacier and to the sides over a distance that scales with the obstacle size and with a smooth fall-off into the fluid, as in the Stokes solution, but this Weertman solution does capture many aspects of the situation.

Then, following Weertman (1957) and Cuffey and Paterson (2010), the classic Weertman solution for the extra stress from creep around obstacles is, for $n = 3$ in the ice flow law,

$$d\sigma_x = \left(\left(9 / 2\right)U / \left(LA\right)\right)^{1/3}, \tag{5}$$

with the creep parameter often taken as $A = 2.4 \times 10^{-24}$ s^{-1} Pa^{-3}. Note that if ice is modeled as linear-viscous so $n = 1$, then A is equivalent to 1/μ, and the Weertman solution yields the same functional dependence for total drag and thus for pressure perturbation near the obstacle as in the Stokes solution, differing only in the geometry and the free-slip Weertman interface versus no-slip Stokes interface. The requirement for high pressure on the upflow side to drive the divergence is quite general, and persists in models going from free-slip to no-slip on the obstacle, and hemispherical to cubic in its shape, for different ice rheologies.

Using the Weertman solution, with ice speed of $U = 100$ m/year (similar to the slowest surface velocity observed in our upglacier survey grid) and $L = 100$ m for an obstacle (typical of the height of many obstacles in the survey

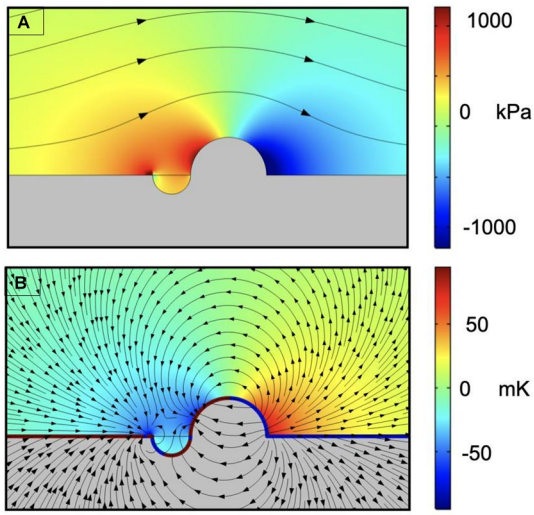

Figure 5. Simulated flow over a bedrock obstacle with stoss-side moat, but with other parameters as in Figure 4. (a) Ice-flow vectors, together with pressure field shown as perturbations with scale bar on right. (b) Heat flow vectors in ice and bed, together with temperature field in ice shown as perturbations with scale bar on right, with the ice-rock interface shown red where there is net heat flow convergence, supporting melting, and blue where there is net heat flow divergence, supporting freezing.

grids) gives $d\sigma_x = 4 \times 10^5$ Pa, and an excess pressure of ice on the bed of more than 10^5 Pa (1 bar). Smaller obstacles or faster sliding would yield larger perturbations, but with smaller obstacles affecting a smaller region (e.g., Lliboutry, 1979, Equation 84). For sufficiently large obstacles, the coupled flow problem with deformation of the free surface becomes important, but any solution will still involve notably enhanced pressure on the stoss side of the obstacle.

3.2. Finite Element Models

To provide further insight to the pressure perturbations caused by flow over basal obstacles, we next return to solutions with linear-viscous ice. MacAyeal (2019) modeled enhanced-creep flow over hemispherical obstacles as well as Weertman-type cuboid "tombstone" obstacles on a horizontal planar bed. Additional simulations have been conducted here, including with stoss-side moats, and we present a few results that we consider to be especially instructive, but these simulations are not intended to exactly model the ice-flow situation at the bed of Thwaites, for reasons discussed below.

3.2.1. Flow Past a Basal Obstacle

Sharp corners in the simulations produce singularities, which are especially evident with the Weertmanian "tombstones" but do not obscure the general features of the solutions (MacAyeal, 2019). All our simulations demonstrate that an obstacle generates a high-pressure perturbation on its stoss side and a low-pressure perturbation on its lee side, and that these pressure perturbations extend, with the same order of magnitude, into the adjacent ice and along the interface with the bed beneath that ice over a distance that scales with the obstacle size. Introducing a stoss-side moat, though, perturbs the stresses, offsetting the pressure perturbations in some ways but amplifying them in others.

As noted by MacAyeal (2019), the results of experiments of this type can be shown nondimensionally, because the perturbations caused by an obstacle scale with the obstacle size. For ease of interpretation, the COMSOL model results here (Figures 4 and 5; also see the Supporting Information S1) are presented dimensionally. MacAyeal (2019) showed three-dimensional simulations; the additional simulations here are two-dimensional (vertical and along-flow; Figure 4a), for simplicity. A linear-viscous fluid ("ice"), with viscosity appropriate for temperate ice (10^{13} Pa s), flows over horizontal, elastic bedrock with one hemispherical protrusion of 100 m radius having properties typical of sedimentary rock. The domain is 4,000 × 4,000 m, centered on the obstacle. The upstream and downstream sides of both ice and rock are periodic for stress balance and temperature, the bottom of the rock is fixed to have zero displacement, and the top of the ice is set at a uniform shear stress of 1 bar (10^5 Pa). The ice/rock interface is constrained to be at the pressure-dependent melting temperature, with free slip on horizontal surfaces, no slip on the bump and on the moat where present, and with the normal force of the ice acting on each segment of the boundary to give the elastic response (no-slip and fully free-slip simulations are given in the Supporting Information S1, as are runs with moats elongated along ice flow; the free-slip/no-slip simulation is shown here because it most closely matches the Stokes solution, and also captures the likely great increase in dynamic drag as ice moves from a soft till to exposed bedrock, where englacial debris likely is abrading the rock, as described below). Thermally, the bottom boundary is insulating, and the temperature on top is set at 273.15 K. We do not independently model a water system between ice and rock, but below we discuss the effects of the pressure perturbations in the ice on a distributed water system. We do not include time-varying boundary conditions (e.g., Wolovick et al., 2014), because of the likelihood that the Thwaites system is fairly close to steady-state in this location that is still well upglacier of the modern grounding zone, as discussed above (e.g., Cuffey et al., 2016; Pollard & DeConto, 2009; Whillans, 1976); we note in Section 6 that some nonsteadiness at small-scale likely is occurring, providing range for further experiments (e.g., Mantelli et al., 2019).

Figure 4b shows the pressure field (the mean of the trace of the stress tensor) in the ice, with ice-flow vectors (the pressure field is also calculated in the elastic bed, but not shown). The pressure satisfies $\nabla^2 P = 0$, in the two separate media. This means that the high pressure of the ice on the stoss side of the bump has a halo of high pressure

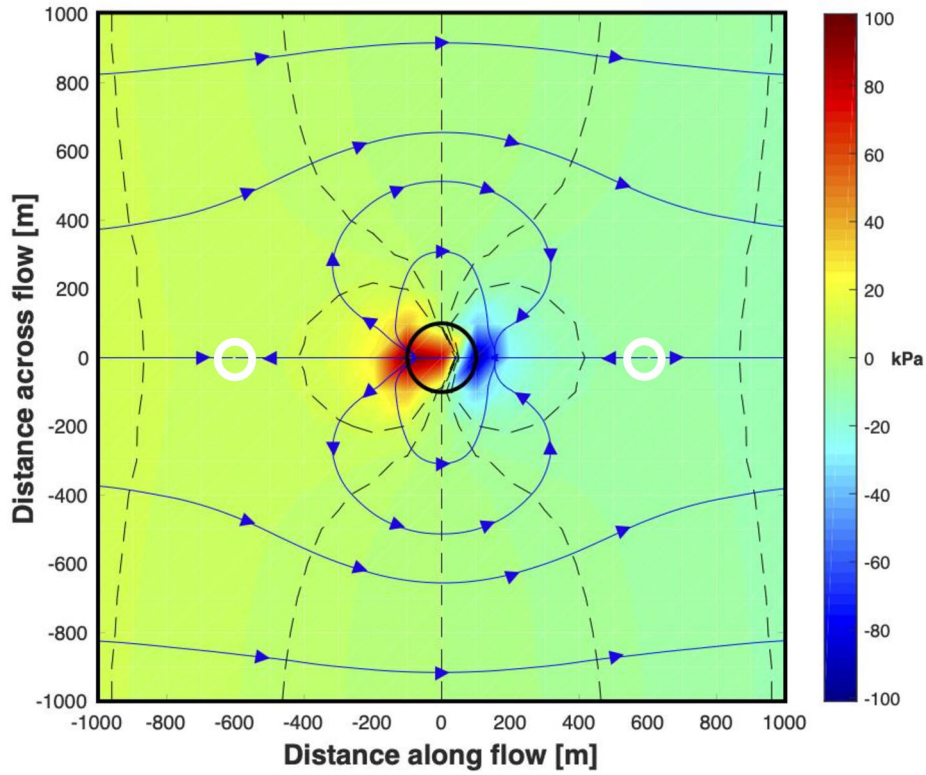

Figure 6. Map-view of basal hydrologic potential (perturbation, shown by color scale and dashed black 5 kPa contours) and water flow lines (blue) for ice flow from left to right, over a 100-m radius obstacle (black circle) centered at (0, 0) on a horizontal bed, assuming the Stokes solution yielding a maximum pressure perturbation of $\sim 10^5$ Pa from viscosity 10^{13} Pa s and 20 m/year ice velocity), a background hydrologic-potential gradient of 10 Pa/m, and water pressure equal to ice pressure, including the perturbation caused by the elevation of the obstacle. The upglacier and downglacier saddle points, as described in the text, are circled in white.

extending upglacier through the ice over a distance that scales with the bump size, which then causes similarly high pressure on the flat part of the bed just upglacier of the bump; equivalent low-pressure regions exist on the lee side. The total stress across the interface is continuous.

The pressure perturbations on the interface maintained at the pressure-dependent melting temperature impose a heat flux to the stoss side of the obstacle and also to the flat part of the bed upglacier of the obstacle in both the ice and the rock, as shown in Figure 4c. Discontinuity of this heat flux is, through the latent heat, the water production/freezing rate. The resulting regelation velocity would be insignificant at this scale, but could be important for smaller bumps, as in MacAyeal (2019) and as discussed further below.

We also conducted model runs (not shown here) introducing a viscous sublayer between ice and rock (viscosity 10^{-4} that of the ice, and thickness 0.1 that of the obstacle radius); this most simply is understood as a till layer, although it might also represent a temperate ice layer between cold ice and rock, or ice softened by included materials. Introducing this layer alters the details of the solutions, and the temperature field is affected slightly depending on whether the pressure-melting criterion is applied at the top or bottom of the viscous sublayer. The pressure perturbations are robust, however, and extend through the ice and the viscous sublayer. Thus, any subglacial till is also subject to the pressure perturbations caused by ice flow against the obstacle.

3.2.2. Flow in the Presence of a Subglacial Moat

In Figure 5, we repeat the simulation from Figure 4 with a crude approximation of a stoss-side moat, here taken as a feature incised into the bed with a semicircular cross-section of radius half that of the obstacle. This increases the maximum pressure perturbation on the obstacle, which is now taller on the stoss side, but, it creates a low-pressure zone in the lee of the upglacier corner of the moat (the green extending just downglacier of the

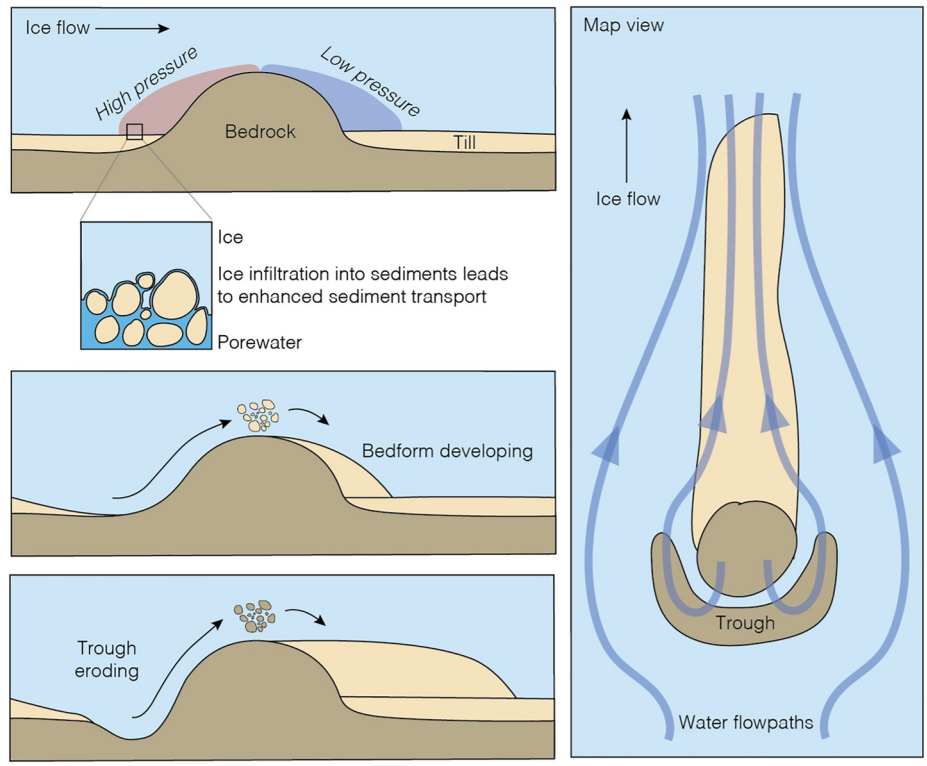

Figure 7. Diagram showing conceptual model for bedform development, as shown in a vertical section along flow (left), from onset of glaciation (top) to modern setting (bottom), which is also shown, together with water-flow paths, in map view on the right.

corner in Figure 5a). This corner acts as an obstacle, the equivalent of a locally high feature interrupting the mean bed sloping down to the bottom of the moat from the upglacier horizontal region. As shown in the Supporting Information S1, switching from this no-slip-obstacle/free-slip-elsewhere to fully free-slip or fully no-slip changes the output in many ways, but preserves these basic features. Interestingly, Clyne et al. (2020) found exposed bedrock in moats, but with "soft" data points in the lee of the lips of the well-sampled moats toward the upglacier end of their seismic line (their Figure 6). This is potentially important in water routing, as discussed below.

One could explore a much wider range of bump sizes and shapes, ice-flow velocities and basal rheologies (including the effects of debris in basal ice) with varying combinations of basal-slip rules for far-field and on-the-bump, and with varying sizes, shapes and sliding laws for moats. A few additional simulations are shown in the Supporting Information S1, but with no intention to span the full possible parameter space. Based on prior work and our simulations to date, rapid ice flow over obstacles will cause perturbations to the basal pressure field near the obstacle that are of the same order of magnitude as the perturbations on the obstacle, over a length that scales with the obstacle size, with compression upglacier, tension downglacier, and the perturbations extending some distance to the side (explored further below, including Figure 6). Furthermore, stoss-side moats have a tendency to offset the influence of obstacles on ice-bed contact pressure over the upglacier part of the moat, with potential implications for subglacial water routing, lubrication, and further moat erosion.

4. Implications for Subglacial Processes Near Basal Obstructions to Flow

4.1. Overview of Subglacial Processes

The robust features of these simulations, combined with the site characteristics of our survey grids, motivate our hypotheses for bedform origin. In this section, we review evidence for the nature of the water and till systems of the survey grids. Some of this information was introduced at least briefly in Muto, Anandakrishnan, et al. (2019), Muto, Alley, et al. (2019), Clyne et al. (2020) or Holschuh et al. (2020); those discussions, and

the discussion here, are supplemented by more-extensive, referenced background information in Text S4 of the Supporting Information S1.

The water system in our study area is distributed and high-pressure, based on the very low acoustic impedance of the tills observed in basins and lee-side positions, as well as on analogy to similar systems elsewhere (Text S4a in the Supporting Information S1). Typical along-flow hydrologic potential gradients in the region are sufficiently small that the large water-pressure perturbations caused by ice flow against obstacles will control ice-contact water flow over distances that scale with obstacle size, as described below. In response, water flowing from far upglacier toward an obstacle on a horizontal bed will be diverted to the sides, remaining well away from the obstacle in all directions (Figures 6 and 7, below). This exclusion of water between ice and bed in a zone upglacier of an obstacle will allow the ice to couple more strongly to the till there (e.g., Rempel, 2008; Zoet & Iverson, 2020), increasing till flux, based on observations at other sites and on models, as described in Text S4b in the Supporting Information S1. In turn, this locally high stoss-side till transport will remove the till there, transferring it downglacier. Some of this till will be deposited in lee-side positions, while the stoss-side removal of till will expose bedrock to erosion that otherwise would be suppressed by the presence of till.

We have described a mechanism by which the pressure gradients resulting from ice flow around a large obstacle drive enhanced erosion. This effect likely occurs at smaller spatial scales as well. Stoss-side high-pressure zones exist for obstacles of all sizes, including abrading clasts. For small clasts (<10 cm), the melting-point depression of the high pressure will drive significant heat convergence to the bed upglacier of the clast that will increase melting there, thus increasing the downward motion of ice past the clast, favoring faster abrasion as described in Text S4c in the Supporting Information S1. The drop in melting temperature as ice approaches the stoss side of a large obstacle should slightly increase abrasion there, also as described in Text S4c in the Supporting Information S1.

4.2. Flow Paths of Water From Upglacier

Water in a distributed ice-contact basal system is typically assumed to flow down the potential gradient arising from variations in bed elevation and ice-surface elevation, with gradients in local effective pressure unimportant over long distances (e.g., Kamb, 2001). Muto, Alley, et al. (2019) and Holschuh et al. (2020) calculated the gradient in the hydrological potential for the distributed water system indicated by seismic and radar data in our study area, assuming a spatially and temporally constant effective pressure. Averaged over the upglacier grid of Figure 1, they found an along-ice-flow gradient of ∼15 Pa/m, with important variations including local reversals over shorter distances, and with the gradient generally of much smaller magnitude over the till-lubricated basins and larger magnitude over the highlands. Thus, ice-pressure perturbations of order 10^5 Pa caused by ice flow against major bumps are large compared to variations over similar length scales caused by ice and bed geometry alone, and compared to any effective pressure that is expected nearby. Such perturbations thus will have major effects on meltwater routing, tending to divert water from upglacier around any obstacles, over a considerable distance that scales with the obstacle size as discussed above (Holschuh et al., 2020).

To illustrate this, in Figure 6 we show the Stokes solution for a 100-m-radius obstacle, with ice viscosity and velocity chosen to yield a maximum pressure perturbation of $\sim 10^5$ Pa, reflective of the Weertman-based calculation above (with ice viscosity $\mu = 10^{13}$ Pa s, this would be 20 m/year ice velocity, or $\mu = 10^{12}$ Pa s and 200 m/year, or any other equivalent combination from Equation 1). Subglacial hydrologic potential contours and flow lines are shown assuming that the water pressure equals the ice pressure or is offset by a constant amount (i.e., constant effective pressure; discussed further below), and that the far-field "background" gradient in ice pressure and thus hydrologic potential is 10 Pa/m, slightly smaller than long-distance average values along Thwaites Glacier but higher than observed gradients in the till-mantled basins of Thwaites Glacier. The Stokes solution would be appropriate for a free-slip boundary away from the bump and a no-slip boundary on the bump in linear-viscous ice, as in Figures 4 and 5. We show a map-plane view of the bed extending 900 m laterally upglacier, downglacier, and across flow from the 100 m obstacle, demonstrating that the perturbations in pressure from ice flow against the obstacle will have a major effect on hydrologic routing extending well beyond the obstacle itself. This in turn will influence till flux, as discussed further in Text S4b in the Supporting Information S1.

As shown in Figure 6, all subglacial water drainage flow paths originating well upglacier remain more than ∼600 m from the center of the obstacle (500 m from the edge). Water flow along the centerline of the obstacle diverges transversely at an upglacier "saddle point" at this distance (Figure 6), converging transversely at the

downglacier saddle point. Closer to the obstacle, any ice-contact water system would be supplied only by the little water generated locally (e.g., by pressure melting, geothermal flux, or heat of sliding close to the obstacle) or by water arriving through a different path (e.g., groundwater flow; see below). With no significant water sink near the lee of the obstacle except for the very small regelation-freeze-on fluxes balancing stoss-side regelation melting, the hydrological potential favors water flow into the lee-side low-pressure zone from all sides, for example, through groundwater, which in turn would tend to raise the water pressure there by displacing ice. The rate of this groundwater flow would depend in important ways on parameters such as bedrock permeability that often are not included in glaciological models. This flow likely would be slow compared to usual subglacial water flow. After onset or reestablishment of glaciation from an initially deglaciated state, this restriction on inflow might allow relatively long-term persistence of a drained bed with low water pressure before formation of lee-side water-filled cavities.

The calculations for Figure 6 assumed a constant effective pressure. Modeling of water flow is further complicated by variations in effective pressure. Weertman (1972; also see Kamb, 1987 and review by R. B. Alley, 1996, among other sources) argued that in the absence of persistent R-channels, steady water pressure decreases and effective pressure increases with increasing basal shear stress. We have been considering the pressure variations across individual obstacles. If one averages over some region of rough bed with numerous small obstacles, the interconnected water will be excluded from stoss sides to accumulate in lee sides. The typical pressure of interconnected water will thus reflect lee-side conditions, and will decrease with increasing shear stress, perhaps more-or-less linearly with a constant of order one. (This influence of basal shear stress on effective pressure is usually assumed to arise from the form drag over the fixed bed and not from interconnection of any cavities formed in the lee of abrading clasts that contribute additional basal shear stress, but we do not know of extensive testing of this idea.) This effect of higher basal shear stress giving lower water pressure cannot cause much change in effective pressure on soft till, however, which cannot support high stoss-side stresses. If water pressure were to be reduced in soft till, ice would tend to regelate into the top of the till (e.g., Meyer et al., 2018), coupling the ice to the till and promoting till deformation and till flux (Text S4b in the Supporting Information S1).

5. Implications for Bedform Development—Stoss-Side Moats

With these insights to the interactions among ice, water and till flows, we return to address moat formation beneath Thwaites Glacier in this section, and then lee-side bedforms in the next section. Our view of formation of these features is shown in the simplified diagram of Figure 7. We recognize that moats may form in other ways than described next, including erosion by flowing water (e.g., Allen, 1971). But, as discussed above, we do not believe that floods can fully explain the widespread, large features observed beneath Thwaites.

The ice sheet originally advanced into a marine basin (Bentley & Ostenso, 1961), where recent, unconsolidated marine sediments must have abutted (and likely extended over, although perhaps in a thinner layer) the bedrock topography. Furthermore, the ice sheet has deglaciated to allow marine sedimentation and then regrown, probably several times although well in the past (e.g., Scherer et al., 1998; reviewed by R. B. Alley et al., 2015). Immediately following glaciation or re-glaciation, the preexisting water-saturated, unconsolidated sediments would have favored low effective pressure, soft-till deformation mostly in thin layers near the base of the ice. But, the higher pressure in the ice generated by the form drag upglacier of a bedrock obstacle would have diverted subglacial water around the obstacle over a distance that scaled with the obstacle size and extended to the sides as well as upglacier (Figure 6). This would have coupled the ice more strongly into the top of the till in those regions (e.g., Iverson & Semmens, 1995; Rempel, 2008), increasing the till flux along ice flow and thus removing the till, exposing bedrock to faster erosion (Cuffey & Alley, 1996) and generating the bedrock-formed stoss-side moats observed today. Transition from soft till on a horizontal surface, to exposed bedrock generating friction during erosion by clasts in ice, with changing topography as moats were eroded, must have affected basal drag with influence on ice-sheet flow, as discussed below.

Despite slight flow divergence, modern ice flow largely continues over the obstacles (Muto, Alley, et al., 2019), as shown by the orientations of the superposed bedforms, by ice-flow modeling, and by analogy to data from deglaciated landscapes. The excess till transported from the upglacier sides of obstacles thus would have been taken over the obstacles to downglacier sides, enabling formation of lee-side bedforms (see below).

Moat formation involves several important feedbacks that will need to be included in a full physical model, as discussed next. We suspect that enough "free parameters" exist that it will be difficult to model their formation from first principles, and some tuning to details of the modern moat form will be required.

Drag from the obstacle will evolve over time, in part based on the relative rate of erosion of the moat versus the surface of the obstacle affecting the relief and shape of the obstacle, but also because of changes in water routing and lubrication. Formation and then deepening of a moat increasingly will direct basal water down into the moat through the effect of the bed slope on the hydrologic potential gradient, opposing the tendency for the excess ice pressure from the bump to drive water away. Also, the growing moat will affect ice flow, causing vertical extension into the moat and associated bridging stresses that reduce the ice-pressure perturbation on the bed, and further reducing ice-contact pressure with the bed as the ice pulls away from the upglacier lip of the moat (see Figure 5a, above). Furthermore, as noted above, the hard bed can sustain a higher effective pressure that scales with the basal shear stress, which also would tend to direct basal water flow into a moat once it has formed.

Ice flow over single small obstacles will not significantly perturb the ice-air surface. For larger obstacles, however, all of the interactions mentioned above are further complicated by the ice-surface response, which depends on the evolving basal topography and lubrication, but which also affects the basal hydrological routing and thus lubrication (e.g., Hiester et al., 2016; Sergienko, 2012). All of this will interact to some degree with large-scale lee-side cavities, discussed next, which influence drainage of basal water past obstacles. Formation of moats thus offers a rich field for future work. Nonetheless, the evidence is strong that initiation of glaciation on a soft-sediment bed with flow against a bedrock obstacle will generate high pressure on the upglacier face and toward the sides of the obstacle over a distance that scales with the obstacle size (Figure 6), more strongly coupling ice to till and increasing till flux, thus removing till and allowing bedrock erosion to produce a stoss-side moat continuing around the sides. Moat erosion includes at least some tendency to be self-limiting, though, with time-evolving influence of the bed form on ice flow, although we do not yet know whether the moats of Thwaites Glacier have approached steady-state.

The observed moats of Thwaites Glacier are as much as 50 m deeper than the surface upglacier, and the limited seismic data suggest that at least some of this relief is eroded into bedrock rather than soft sediment. Even a small excess stoss-side erosion rate can explain that much relief over the million-year timescale since formation of the West Antarctic Ice Sheet.

6. Implications for Bedform Development—Lee-Side Features

6.1. Lee-Side Lineations

The bed of Thwaites includes elongated, soft-sediment bedforms extending at least ∼15 km along ice flow in the lee of bedrock bumps (crag-and-tail features). These flutes (or tails of crag-and-tail features, or mega-scale glacial lineations, or whatever terminology is adopted) taper and drop in elevation only slightly over that length, until encountering another geological boundary with moats upglacier of bedrock bumps. Arguably, some of the flutes continue in reduced form across the geological boundary. But, even if they do not continue, the form of the flutes suggests that they would be much longer if the geological boundary were farther downglacier.

The flutes are up to 100 m high, and are seismically soft on top, indicating water pressure very close to overburden pressure, hence small effective pressure N. The troughs between flutes also have small N, but the limited data suggest that N is generally larger in troughs than on crests. One might expect, however, that the difference in density between ice and water would cause N to be much larger on crests than on troughs—based purely on hydrostatic considerations, water should drain away from crests. Seismically "soft" crests of elongated bedforms have also been observed beneath Rutford Ice Stream (Smith et al., 2007) and the Northeast Greenland Ice Stream (Riverman et al., 2019), and Barcheck et al. (2020) observed clustering of seismicity in troughs beneath Whillans Ice Stream, suggesting a stronger bed there than on crests.

Either erosion or sedimentation separately, or both acting together, could create such streamlined lee-side bedforms. For Thwaites, it is likely that both are involved.

Looking first at erosion, the combined seismic and radar data (Figures 1 and 2; see the downglacier highlands of Figure 6 in Clyne et al., 2020, and the highlands in Muto, Anandakrishnan, et al., 2019) show some upland regions with streamlined bedforms that have high acoustic impedances indicating sedimentary bedrock rather

than material deposited recently by Thwaites Glacier. Hence, we can conclude that erosion has contributed to formation of the bedforms in at least part of our survey area.

We consider it highly likely that at least some of the "soft" materials in lee-side positions were deposited there by glacial action rather than being entirely sculpted by erosion of unlithified preglacial sediments. Arguments for this depositional origin are suggestive rather than conclusive, however, and motivate targeted investigations.

The soft-topped, lee-side bedforms are as much as 100 m high, and soft sediment likely continues beneath the inter-ridge troughs at least in some places (Figure 3), so if the bedforms were entirely shaped by erosion, the preexisting sediment drape must have been at least 100 m thick. High-resolution West Antarctic seismic surveys often identify reflectors in the top 100 m of sub-ice-bottom sediments (e.g., Peters et al., 2006; Rooney et al., 1987), so the absence of such reflectors here is at least suggestive that the bedforms were not entirely eroded from extensive preexisting sedimentary layers. More-detailed surveys to study the internal structure of the bedforms would be of interest, looking for horizontal layering versus prograding layering from lee-side sedimentation (also see Riverman et al., 2019).

Erosion of bedrock generally produces rough surfaces at multiple wavelengths (e.g., Boulton, 1979; Iverson, 2012), reflecting inhomogeneity in the rock or its fracture patterns, together with the rock being strong enough to support this roughness against the ice-flow stresses. Lee-side soft-sediment accumulations are widespread in our survey grids. One might expect that erosion sufficient to sculpt 100-m-high features in the lowlands would have produced new roughness elements lacking inherited sediments in the highlands, or would have removed all the inherited sediment from many of the roughness elements in the highlands.

Based on these considerations, on the long-standing conviction among glaciologists and glacial geologists that lee-side sedimentation does occur (e.g., Fowler, 2010; Lliboutry, 1958), the documented growth of a bedform under Rutford Ice Stream (Smith et al., 2007), and the observations presented here, it appears highly likely that the bedforms of Thwaites were formed by lee-side sedimentation as well as by erosion, although we cannot prove this with available data. In this view, erosion has occurred in the highlands and in troughs in the lowlands, with deposition in lee-side positions in highlands and lowlands. Bedforms then comprise eroded "crags" at the upglacier end, eroded troughs and flanks, and till deposited higher on flanks and beneath crests in lee-side positions. Analogy can be drawn to drumlins, which in at least some cases have such a compound erosional-depositional origin (e.g., McCracken et al., 2016; Whittecar & Mickelson, 1977; Woodard et al., 2020).

6.2. Lee-Side Cavities

The lee-side bedforms considered here are impressive in their height, width, and length, and in total are among the more spectacular observed glacially streamlined features. The site characteristics, however, are unremarkable, except for the long-term persistence of glaciation. Ice-flow velocity is modest (90–150 m/yr in the upglacier grid, 300–400 m/yr in the downglacier grid), with the bedforms generally somewhat longer in the lower-velocity upglacier region than in the higher-velocity downglacier region (contrary to some models; Holschuh et al., 2020). We suggest that the persistence of glaciation in our survey grids has been the most important contributor to the great length of the well-defined bedforms we observe. This in turn suggests that many bedforms from deglaciated terrains of, for example, the Laurentide and Fennoscandian ice sheets, had not reached steady state and so would have continued to evolve if glaciation had persisted. This surely is not a new idea, but we develop it a little below, suggesting that nonsteadiness may be important in the evolution of ice flow as well as bed character.

As noted above, research at least since Stokes (1851) on flow past an obstacle has shown that a stoss-side high-pressure zone is paired with a lee-side low-pressure zone. In the subglacial system, water-filled cavities often form in those lee-side positions, and have long been integral in major treatments of basal sliding (e.g., Fowler, 2010; Schoof, 2005). Here, we are interested in the length of such cavities relative to the length of observed bedforms because it provides a partial constraint on the origin of bedforms, but this poses some difficulties. As discussed next, the most commonly used model for subglacial-cavity length suggests that the observed bedforms could have formed by sedimentation in preexisting water-filled cavities that initially were as long as, or longer than, the modern bedforms; however, additional considerations suggest instead that the initial cavities would have been shorter than the observed bedforms, which reached their full length by prograding sedimentation (also see Ives & Iverson, 2019).

In the most commonly used physical model for lee-side water-filled cavities, their lengths are calculated by balancing the rate of cavity opening through ice flow and cavity-roof melting against the rate of creep closure in response to effective pressure N (Walder, 1986). Ignoring melting of the cavity roof (which is generally small, but which, if included, would make the cavity longer), the cavity length L then is (Cuffey & Paterson, 2010):

$$L = U \Big/ \left[A\left(N \Big/ n\right)^n \right] \tag{6}$$

for basal-ice-flow velocity U, power-law deformation of ice with prefactor A (often taken as $A = 2.4 \times 10^{-24}$ s^{-1} Pa^{-3} for ice at the melting point, following Cuffey & Paterson, 2010), and power $n = 3$. As noted by Cuffey and Paterson (2010), L can become very large at small effective pressure N. For an effective pressure of 0.1 bar = 10^4 Pa, for example, a possible sub-ice-sheet value (see above), a velocity of ~110 m/year gives cavity-length L equal to the circumference of the Earth. This clearly is absurd. A more-complete flow law for ice including linear as well as power-law processes would estimate somewhat faster closure and thus somewhat shorter cavities, but still orders of magnitude longer than the observed bedforms.

The modeling work of Barchyn et al. (2016) highlights this difficulty. They used a heuristic set of equations for basal processes, including this Walder (1986)-type control on cavity length assuming linear-viscous ice, to simulate realistic-looking bedforms matching observed dimensions of drumlins and other features of deglaciated terrains; however, these results were obtained by setting the effective pressure $N = 5$ MPa, equivalent to air-filled lee-side cavities under more than 500 m of ice. Reducing that effective pressure by two orders of magnitude or more to match sub-ice-sheet conditions of Thwaites Glacier would yield cavities two orders of magnitude longer or more in this linear model, with a greater difference if cubic power-law deformation were used.

As noted in the discussion of the water system, Figure 6 suggests another process that places a much more restrictive limit on the length of steady-state lee-side water-filled cavities, likely shorter than the observed bedforms; this in turn implies that the long observed bedforms formed by sustained prograding sedimentation rather than by infilling of a preexisting long cavity. In this simple example, groundwater flow will supply basal water to the lee-side position until the water pressure exceeds the value at the saddle point and the water-filled cavity with its single water pressure extends past the saddle point. Leakage from the downglacier end of the cavity into the adjacent lower-pressure distributed water system then will limit further cavity growth. Total cavity length thus may tend to be limited to somewhat longer than (approximately twice?) the distance to the saddle point, so that water loss downglacier of the saddle point balances water inflow upglacier of the saddle point.

Clearly, as a cavity grows, it will disturb the pressure field, basal lubrication, and, for large obstacles, the ice-air surface, so the distance to the saddle point cannot be a fixed value. Nonetheless, the scaling here may be useful. Ice-marginal regions with steep potential gradients might have relatively short steady cavities, whereas inland regions with low potential gradients will not. This will interact with sliding speeds, which are lower inland, favoring smaller pressure perturbations across an obstacle and thus shorter cavities. This limit on cavity length seems likely to give water-filled cavities significantly shorter than the longest observed bedforms in our survey or in some other regions, suggesting that long bedforms may have reached that length not by sediment filling a long preexisting cavity, but by filling a shorter cavity (or forming without a cavity) and then extending downglacier by prograding sedimentation (see, e.g., Ives & Iverson, 2019; Zoet et al., 2021).

6.3. Lee-Side Sedimentation

Sedimentation in lee-side cavities thus is important in our hypothesis. Seismic surveys reveal extensive lee-side bedforms today, but only restricted water-filled lee-side cavities (Clyne et al., 2020; Muto, Anandakrishnan, et al., 2019). Presuming our hypothesis is correct, we do not know whether water-filled lee-side cavities formed and then filled with sediment, or whether the ice-bedrock separation developed concurrent with sedimentation. The Bentley and Ostenso (1961; also see Lindstrom, 1988) hypothesis that the West Antarctic Ice Sheet formed by thickening of an ice shelf suggests that the ice grounded first on the high zones of the bed, which may have produced sub-ice-shelf tidal channels in the lee of bedrock highs (K. E. Alley et al., 2016; Horgan et al., 2013), which then filled with sediment as the ice grounded. One can, however, imagine very different histories for Thwaites Glacier, and for other ice sheets. For example, a cold-based ice cap that grows until the bed thaws would have very

limited basal water initially, and might not be able to fill lee-side cavities rapidly with the available water, giving a different history than for grounding of an ice shelf.

As noted above (also see Muto, Alley, et al., 2019), basal ice flow primarily continues across basal topography despite some flow deflection. In a sedimentary basin well upglacier of a basal obstacle, small hydrologic-potential gradients lead to inefficient water drainage, partially decoupling the ice from the bed, so deforming till flux is small although nonzero. The high-pressure perturbation on the stoss side of an obstacle increases ice-till coupling and till deformation there, leading to thinning of the deforming till layer onto the obstacle, and likely producing till discontinuity in space or time. If there were a lee-side cavity, this sediment would be deposited on the lee side, building up to contact the ice roof of the cavity. Steady state could be reached when the ice-till coupling on the lee side matched the ice-till coupling well upglacier of the obstacle, as required by till mass-balance considerations along with the dependence of till transport rates on coupling. For Thwaites, the upglacier region has soft till and high water pressure with weak coupling between ice and till, so similarly soft till weakly coupled to the ice is required downglacier of the obstacle. (Clearly, ice, water, and till fluxes and ice velocity evolve along flow, so lee-side and stoss-side conditions are not identical, but because the survey sites are well downglacier from the ice divide, the flux and velocity changes across any one obstacle are small compared to the mean values.)

Counterfactually, if the crest of a lee-side bedform were well-drained, the ice then would be well-coupled to the till there, till flux would be higher than the supply from upglacier of the obstacle, and the crest of the bedform would be eroded until partial decoupling was achieved. Similarly, if the crest of the lee-side bedform were less-well coupled to the ice than in upglacier regions, till flux along the lee-side bedform would be less than supply from upglacier, and till would build up to raise the crest of the bedform. The steady-state condition must be maintained with transverse groundwater flow, which may influence aspect ratios of the dominant bedforms that develop. The water supplied to the low-pressure lee-side region from the surroundings leaves them less well lubricated, favoring the slightly "harder" beds in troughs, with the concentrated microseismicity observed by Barcheck et al. (2020).

In this picture, the rate of bedform elongation is the ratio of the sediment flux from upglacier to the bedform height. Figure 1 shows bedforms beneath Thwaites extending at least to the moats generated by the next structurally controlled bedrock highs, although as noted above, reduced-amplitude bedforms likely extend even farther. In the absence of a bedrock high, the bedforms might be limited by along-flow variations in the ice sheet (a steady bedform cannot emerge above the downward-sloping ice surface, for example), but very long bedforms are possible given enough integrated sediment flux, which increases with persistence of glaciation.

6.4. Lee-Side Moats?

In several places in the upglacier and downglacier grids in Figure 2, there are features that can be interpreted as lee-side moats (see, e.g., the lower-left corner of Figure 2d). In most cases, these could also be seen as stoss-side moats for obstacles farther downglacier, but there are hints of lee-side moats. We can think of at least three possible explanations. The easiest might be lithologic control, such as a more-or-less circular volcanic plug with an easily erodible alteration halo, but there seems to be little independent evidence to support this. Perhaps more likely, the difficulty of lubricating water reaching lee-side positions, as described above, may have caused strong coupling between ice and till in lee-side positions shortly after the onset of glaciation and lasting long enough for some lee-side moat erosion before sufficient inflow of water to separate ice from till. And, perhaps most likely, this part of Thwaites Glacier might initially have been glaciated by ice advancing from the nearby Amundsen Sea rift flank and eroding stoss-side moats, followed by flow reversal to the modern pattern as the ice sheet built up across the deep basins to the south (Lindstrom, 1988; Pollard & DeConto, 2009); some such moats might have been eroded away or buried by sediment since formation, and all would have been initially small because of the short duration of the reversed flow.

7. Synthesis

Onset and subsequent reestablishment of glaciation at Thwaites Glacier likely occurred by grounding of an ice shelf (Bentley & Ostenso, 1961), as noted above, with great uncertainty as to what happened in detail, and even which way the grounded ice flowed initially (Lindstrom, 1988). The first grounding or regrounding of ice would have occurred on a drape of unconsolidated sediment, which likely was thicker in basins and thinner over

topographic highs, and initially with no glacially carved moats or lee-side deposits. Erosion of the thinner and more-exposed sediments on the highlands would have exposed the sedimentary bedrock, while soft-sediment layers persisted in lowlands. Soft-sediment layers lubricate ice flow efficiently, giving low surface slopes and driving stresses, and supporting a distributed water system with pressure close to the overburden.

Ice flow from well-lubricated basins against highlands generates stoss-side high-pressure and lee-side low-pressure zones extending to the sides of the obstacle as well, and extending into the ice and against the bed over a distance that scales with the obstacle size, and with large enough magnitude to redirect subglacial water flow (Figure 7). On the stoss side of an obstacle, this excludes subglacial water and couples the ice more strongly to the till, allowing the ice to more efficiently transport that till to the lee side and then erode a stoss-side moat into the subjacent bedrock and extending to the sides of the obstacle. During bedrock erosion to form moats, the drag will be enhanced compared to the initial till-lubricated bed or the subsequent water-lubricated bed after the moat has redirected water into it. Hence, resistance to ice flow is expected to evolve notably over time.

On the lee side, the low-pressure zone may initially lack an efficient water supply because the water is routed well around the obstacle; groundwater flow may be important. Eventually, any water-filled cavities that form may be limited in length by downglacier leakage to the sides where the far-field water potential is lower than that in the cavity. Steeper far-field hydrologic potential gradients then give shorter maximum cavity lengths. Sediment transported over obstacles will be deposited in lee-side cavities or in lee-side positions even in the absence of cavities, and can prograde downglacier to great lengths if glaciation is maintained for a long enough time, at a rate that depends on sediment supply from upglacier. Tops of such lee-side deposits must be soft, as observed, to approach steady-state with ice-till coupling similar to that in the till-mantled basin well upglacier of the obstacle. Erosion of moats may allow water flow through them to more efficiently reach lee-side deposits.

Much work is required to develop, test, and extend the hypotheses presented here. Coupled modeling appears especially important, including ice with free-surface response (e.g., Sergienko, 2012, 2013; Whillans & Johnsen, 1983), nonsteady water flow, till deformation, bedrock erosion, and redirection of subglacial distributed water under the pressure perturbations from ice as well as the influence of varying basal shear stress (e.g., Hiester et al., 2016).

Analogy to Rutford Ice Stream suggests that sediment transport may be notably nonsteady, further complicating modeling (Smith et al., 2007; cf. Davies et al., 2018). The existence of seismically thick water in some places beneath Thwaites (Clyne et al., 2020; Muto, Anandakrishnan, et al., 2019) suggests nonsteadiness; persistent thick water likely would have been filled by sediment over the lifespan of the ice sheet. The observed subglacial lake drainages of Thwaites (Hoffman et al., 2020; Smith et al., 2017), although geographically restricted, also show local nonsteadiness. Ice flowing across a till-mantled sedimentary basin has an ice-contact water system, low effective pressure N, poor ice-till coupling, and low till transport rates, enabling persistence of till within the basin over the lifespan of the ice sheet to date, but with spatial variability that is important to both ice and bedform dynamics.

The ice that reaches a bedrock obstacle primarily flows over it, while the water is diverted around, and that water must reestablish a drainage system; this creates a situation that is nonsteady in a Lagrangian frame of reference moving with the basal ice, and poses additional challenges for modeling the reestablishment of a distributed system. These and more issues likely will need to be considered. We suspect that inverting models for parameters to fit mapped bedforms will be important in moving forward to understand this complex system.

We are hopeful that these results provide insights to the formation of bedforms elsewhere. We are particularly interested in the role of nonsteadiness in controlling bedforms, and of bedforms in controlling ice flow.

Appendix A

Members of the Geophysical Habitat of Subglacial Thwaites (GHOST) Collaboration team are Andy Smith, Rob Arthern, Robert Bingham, Alex Brisbourne, Olaf Eisen, Coen Hofstede, Bernd Kulessa, Leigh Sterns, Paul Winberry, Julien Bodart, Louise Borthwick, Elizabeth Case, Chloe Gustafson, Jonny Kingslake, Helen Ockenden, Charlotte Schoonman, and Emily Schwans.

Conflict of Interest

The authors declare no conflicts of interest relevant to this study.

Data Availability Statement

The seismic and radar data for this study were published with the papers cited. Additional details of the simulations conducted as well as additional simulations are discussed in the Supporting Information S1; the simulation data are archived and freely available at http://www.datacommons.psu.edu/commonswizard/MetadataDisplay.aspx?Dataset=6181 also linked at https://doi.org/10.26208/ce9f-sm73. We thank colleagues at the Center for Remote Sensing of Ice Sheets (CReSIS) and the International Thwaites Glacier Collaboration (ITGC).

Acknowledgments
This research was supported by the U.S. National Science Foundation under grants AGS-1338832, NSF-NERC-OPP-1738934 and by the Heising-Simons Foundation under grant 2018-0769.

References

Allen, J. R. L. (1971). Transverse erosional marks of mud and rock: Their physical basis and geological significance. *Sedimentary Geology*, *5*(3–4), 167–385. https://doi.org/10.1016/0037-0738(71)90001-7

Alley, K. E., Scambos, T. A., Alley, R. B., & Holschuh, N. D. (2019). Troughs developed in ice-stream shear margins precondition ice shelves for ocean-driven breakup. *Science Advances*, *5*(10), 7. https://doi.org/10.1126/sciadv.aax2215

Alley, K. E., Scambos, T. A., Siegfried, M. R., & Fricker, H. A. (2016). Impacts of warm water on Antarctic ice shelf stability through basal channel formation. *Nature Geoscience*, *9*, 290–293. https://doi.org/10.1038/ngeo2675

Alley, R. B. (1996). Towards a hydrological model for computerized ice-sheet simulations. *Hydrologic Processes*, *10*, 649–660. https://doi.org/10.1002/(SICI)1099-1085(199604)10:4<649::AID-HYP397>3.0.CO;2-1

Alley, R. B., Anandakrishnan, S., Christianson, K., Horgan, H. J., Muto, A., Parizek, B. R., et al. (2015). Oceanic forcing of ice-sheet retreat: West Antarctica and more. *Annual Review of Earth and Planetary Sciences*, *43*, 207–231. https://doi.org/10.1146/annurev-earth-060614-105344

Alley, R. B., Cuffey, K. M., & Zoet, L. K. (2019). Glacial erosion: Status and outlook. *Annals of Glaciology*, *60*(80), 1–13. https://doi.org/10.1017/aog.2019.38

Alley, R. B., Dupont, T. K., Parizek, B. R., Anandakrishnan, S., Lawson, D. E., Larson, G. J., & Evenson, E. B. (2006). Outburst flooding and the initiation of ice-stream surges in response to climatic cooling: A hypothesis. *Geomorphology*, *75*(1–2), 76–89. https://doi.org/10.1016/j.geomorph.2004.01.011

Barcheck, C. G., Schwartz, S. Y., & Tulaczyk, S. (2020). Icequake streaks linked to potential mega-scale glacial lineations beneath an Antarctic ice stream. *Geology*, *48*, 99–102. https://doi.org/10.1130/G46626.1

Barchyn, T. E., Dowling, T. P. F., Stokes, C. R., & Hugenholtz, C. H. (2016). Subglacial bed form morphology controlled by ice speed and sediment thickness. *Geophysical Research Letters*, *43*, 7572–7580. https://doi.org/10.1002/2016GL069558

Behrendt, J. C. (1999). Crustal and lithospheric structure of the West Antarctic Rift System from geophysical investigations—A review. *Global and Planetary Change*, *23*(1–4), 25–55. https://doi.org/10.1016/S0921-8181(99)00049-1

Bentley, C. R. (1987). Antarctic ice streams: A review. *Journal of Geophysical Research*, *92*(B9), 8843–8858. https://doi.org/10.1029/JB092iB09p08843

Bentley, C. R., & Ostenso, N. A. (1961). Glacial and subglacial topography of West Antarctica. *Journal of Glaciology*, *3*(29), 882–912. https://doi.org/10.3189/S0022143000027271

Bingham, R., Ferraccioli, F., King, E., Larter, R. D., Pritchard, H. D., Smith, A. M., & Vaughan, D. G. (2012). Inland thinning of West Antarctic Ice Sheet steered along subglacial rifts. *Nature*, *487*, 468–471. https://doi.org/10.1038/nature11292

Bingham, R. G., Vaughan, D. G., King, E. C., Davies, D., Cornford, S. L., Smith, A. M., et al. (2017). Diverse landscapes beneath Pine Island Glacier influence ice flow. *Nature Communications*, *8*, 1618. https://doi.org/10.1038/s41467-017-01597-y

Boulton, G. S. (1979). Processes of glacier erosion on different substrata. *Journal of Glaciology*, *23*(89), 15–37. https://doi.org/10.3189/S0022143000029713

Childress, S. (2009). *An introduction to theoretical fluid mechanics*. Courant Institute of Mathematical Sciences.

Christianson, K., Peters, L. E., Alley, R. B., Anandakrishnan, S., Jacobel, R. W., Riverman, K. L., et al. (2014). Dilatant till facilitates ice-stream flow in northeast Greenland. *Earth and Planetary Science Letters*, *401*, 57–69. https://doi.org/10.1016/j.epsl.2014.05.060

Clyne, E. R., Anandakrishnan, S., Muto, A., Alley, R. B., & Voigt, D. E. (2020). Reflection seismic interpretation of topography and acoustic impedance beneath Thwaites Glacier, West Antarctica. *Earth and Planetary Science Letters*, *550*, 116543. https://doi.org/10.1016/j.epsl.2020.116543

Cuffey, K. M., & Alley, R. B. (1996). Erosion by deforming subglacial sediments: Is it significant? (toward till continuity). *Annals of Glaciology*, *22*, 126–133. https://doi.org/10.3189/1996AoG22-1-17-24

Cuffey, K. M., Clow, G. D., Steig, E. J., Buizert, C., Fudge, T. J., Koutnik, M., et al. (2016). Deglacial temperature history of West Antarctica. *Proceedings of the National Academy of Sciences of the United States of America*, *113*(50), 14249–14254. https://doi.org/10.1073/pnas.1609132113

Cuffey, K. M., & Paterson, W. S. B. (2010). *The physics of glaciers* (4th ed.). Butterworth-Heinemann.

Davies, D., Bingham, R. G., Graham, A. G. C., Spagnolo, M., Dutrieux, P., Vaughan, D. G., et al. (2017). High-resolution sub-ice-shelf seafloor records of twentieth century ungrounding and retreat of Pine Island Glacier, West Antarctica. *Journal of Geophysical Research: Earth Surface*, *122*, 1698–1714. https://doi.org/10.1002/2017JF004311

Davies, D., Bingham, R. G., King, E. C., Smith, A. M., Brisbourne, A. M., Spagnolo, M., et al. (2018). How dynamic are ice-stream beds? *The Cryosphere*, *12*, 1615–1628. https://doi.org/10.5194/tc-12-1615-2018

DeConto, R. M., & Pollard, D. (2016). Contribution of Antarctica to past and future sea-level rise. *Nature*, *531*, 591–597. https://doi.org/10.1038/nature17145

Drewry, D. J., Jordan, S. R., & Jankowski, E. (1983). Measured properties of the Antarctic ice sheet: Surface configuration, ice thickness, volume and bedrock characteristics. *Annals of Glaciology*, *3*, 83–91. https://doi.org/10.3189/S0260305500002573

Fowler, A. C. (2010). Weertman, Lliboutry and the development of sliding theory. *Journal of Glaciology*, *56*(200), 965–972. https://doi.org/10.3189/002214311796406112

Fretwell, P., Pritchard, H. D., Vaughan, D. G., Bamber, J. L., Barrand, N. E., Bell, R., et al. (2013). Bedmap2: Improved ice bed, surface and thickness datasets for Antarctica. *The Cryosphere*, *7*, 375–393. https://doi.org/10.5194/tc-7-375-2013

Hiester, J., Sergienko, O. V., & Hulbe, C. L. (2016). Topographically mediated ice stream subglacial drainage networks. *Journal of Geophysical Research: Earth Surface*, *121*, 497–510. https://doi.org/10.1002/2015JF003660

Hoffman, A. O., Christianson, K., Shapero, D., Smith, B. E., & Joughin, I. (2020). Brief communication: Heterogenous thinning and subglacial lake activity on Thwaites Glacier, West Antarctica. *The Cryosphere Discussions*. https://doi.org/10.5194/tc-2020-80

Holschuh, N., Christianson, K., Paden, J., Alley, R. B., & Anandakrishnan, S. (2020). Linking postglacial landscapes to glacier dynamics using swath radar at Thwaites Glacier. *Geology*, *48*, 268–272. https://doi.org/10.1130/G46772.1

Horgan, H. J., Alley, R. B., Christianson, K., Jacobel, R. W., Anandakrishnan, S., Muto, A., et al. (2013). Estuaries beneath ice sheets. *Geology*, *41*(11), 1159–1162. https://doi.org/10.1130/G34654.1

Iverson, N. (2012). A theory of glacial quarrying for landscape evolution models. *Geology*, *40*(8), 679–682. https://doi.org/10.1130/G33079.1

Iverson, N. R., & Semmens, D. J. (1995). Intrusion of ice into porous media by regelation: A mechanism of sediment entrainment by glaciers. *Journal of Geophysical Research*, *100*(B7), 10,219–10,230. https://doi.org/10.1029/95JB00043

Ives, L. R. W., & Iverson, N. R. (2019). Genesis of glacial flutes inferred from observations at Múlajökull, Iceland. *Geology*, *47*, 1–4. https://doi.org/10.1130/G45714.1

Johnson, J. S., Smith, J. A., Schaefer, J. M., Young, N. E., Goehring, B. M., Hillenbrand, C.-D., et al. (2017). The last glaciation of Bear Peninsula, central Amundsen Sea Embayment of Antarctica: Constraints on timing and duration revealed by in situ cosmogenic 14C and 10Be dating. *Quaternary Science Reviews*, *178*, 77–88. https://doi.org/10.1016/j.quascirev.2017.11.003

Joughin, I., Smith, B. E., & Medley, B. (2014). Marine ice sheet collapse potentially under way for the Thwaites Glacier Basin, West Antarctica. *Science*, *344*(6185), 735–738. https://doi.org/10.1126/science.1249055

Kamb, B. (1987). Glacier surge mechanism based on linked cavity configuration of the basal water conduit system. *Journal of Geophysical Research*, *92*(B9), 9083–9100. https://doi.org/10.1029/JB092iB09p09083

Kamb, B. (2001). Basal zone of the West Antarctic ice streams and its role in lubrication of their rapid motion. In R. B. Alley, & R. A. Bindschadler (Eds.), *The West Antarctic ice sheet: Behavior and environment, Antarctic research series* (Vol. 77, pp. 157–199). American Geophysical Union. https://doi.org/10.1029/AR077p0157

King, E., Hindmarsh, R., & Stokes, C. (2009). Formation of mega-scale glacial lineations observed beneath a West Antarctic ice stream. *Nature Geoscience*, *2*, 585–588. https://doi.org/10.1038/ngeo581

Kingslake, J., Scherer, R. P., Albrecht, T., Coenen, J., Powell, R. D., Reese, R., et al. (2018). Extensive retreat and re-advance of the West Antarctic Ice Sheet during the Holocene. *Nature*, *558*, 430–434. https://doi.org/10.1038/s41586-018-0208-x

Kirkham, J. D., Hogan, K. A., Larter, R. D., Arnold, N. S., Nitsche, F. O., Golledge, N. R., & Dowdeswell, J. A. (2019). Past water flow beneath Pine Island and Thwaites glaciers, West Antarctica. *The Cryosphere*, *13*, 1959–1981. https://doi.org/10.5194/tc-13-1959-2019

Koellner, S., Parizek, B. R., Alley, R. B., Muto, A., & Holschuh, N. (2019). The impact of spatially-variable basal properties on outlet glacier flow. *Earth and Planetary Science Letters*, *515*, 200–208. https://doi.org/10.1016/j.epsl.2019.03.026

Lindstrom, D. R. (1988). Formation of the west Antarctic ice sheet. *Annals of Glaciology*, *11*, 71–76. https://doi.org/10.3189/S0260305500006352

Lliboutry, L. (1958). Contribution a` la théorie du frottement du glacier sur son lit. *Comptes Rendus Hebdomadaires des Seances de l'Academie des Sciences*, *247*(3), 318–320.

Lliboutry, L. (1979). Local friction laws for glaciers: A critical reviewand new openings. *Journal of Glaciology*, *23*(89), 67–95. https://doi.org/10.3189/S0022143000029750

MacAyeal, D. R. (2019). Revisiting Weertman's tombstone bed. *Annals of Glaciology*, *60*(80), 1–9. https://doi.org/10.1017/aog.2019.31

Malczyk, G., Gourmelen, N., Goldberg, D., Wuite, J., & Nagler, T. (2020). Repeat subglacial lake drainage and filling beneath Thwaites Glacier. *Geophysical Research Letters*, *47*, e2020GL089658. https://doi.org/10.1029/2020GL089658

Mantelli, E., Haseloff, M., & Schoof, C. (2019). Ice sheet flow with thermally activated sliding. Part 1: The role of advection. *Proceedings of the Royal Society A*, *475*, 20190410. https://doi.org/10.1098/rspa.2019.0410

McCracken, R. G., Iverson, N. R., Benediktsson, Í. Ö., Schomacker, A., Zoet, L. K., Johnson, M. D., et al. (2016). Origin of the active drumlin field at Múlajökull, Iceland: New insights from till shear and consolidation patterns. *Quaternary Science Reviews*, *148*, 243–260. https://doi.org/10.1016/j.quascirev.2016.07.008

Menzies, J. (1984). *Drumlins: A bibliography. Geo abstracts bibliography No. 15* (p. 117). Norwich Publishing.

Meyer, C. R., Downey, A. S., & Rempel, A. W. (2018). Freeze-on limits bed strength beneath sliding glaciers. *Nature Communications*, *9*, 3242. https://doi.org/10.1038/s41467-018-05716-1

Millilo, P., Rignot, E., Rizzoli, P., Scheuchl, B., Mouginot, J., Bueso-Bello, J., & Rrats-Iraola, P. (2019). Heterogeneous retreat and ice melt of Thwaites Glacier, West Antarctica. *Science Advances*, *5*, eaau3433. https://doi.org/10.1126/sciadv.aau3433

Morlighem, M., Rignot, E., Binder, T., Blankenship, D., Drews, R., Eagles, G., et al. (2020). Deep glacial troughs and stabilizing ridges unveiled beneath the margins of the Antarctic ice sheet. *Nature Geoscience*, *13*, 132–137. https://doi.org/10.1038/s41561-019-0510-8,2019

Muto, A., Alley, R. B., Parizek, B. R., & Anandakrishnan, S. (2019). Bed-type variability and till (dis)continuity beneath Thwaites Glacier, West Antarctica. *Annals of Glaciology*, *60*(80), 1–9. https://doi.org/10.1017/aog.2019.32

Muto, A., Anandakrishnan, S., & Alley, R. B. (2013). Subglacial bathymetry and sediment layer distribution beneath the Pine Island Glacier ice shelf, West Antarctica, modeled using aerogravity and autonomous underwater vehicle data. *Annals of Glaciology*, *54*(64), 27–32. https://doi.org/10.3189/2013aog64a110

Muto, A., Anandakrishnan, S., Alley, R. B., Horgan, H. J., Parizek, B. R., Koellner, S., et al. (2019). Relating bed character and subglacial morphology using seismic data from Thwaites Glacier, West Antarctica. *Earth and Planetary Science Letters*, *507*, 199–206. https://doi.org/10.1016/j.epsl.2018.12.008

OECD. (2015). Road traffic, vehicles and networks. In *Environment at a glance 2015: OECD indicators*. : OECD Publishing. https://doi.org/10.1787/9789264235199-17-en

Parizek, B. R., Christianson, K., Anandakrishnan, S., Alley, R. B., Walker, R. T., Edwards, R. A., et al. (2013). Dynamic (in)stability of Thwaites Glacier, West Antarctica. *Journal of Geophysical Research: Earth Surface*, *118*, 1–18. https://doi.org/10.1002/jgrf.20044

Peters, L. E., Anandakrishnan, S., Alley, R. B., Winberry, J. P., Voigt, D. E., Smith, A. M., & Morse, D. L. (2006). Subglacial sediments as a control on the onset and location of two Siple Coast ice streams, West Antarctica. *Journal of Geophysical Research*, *111*(B1), B01302. https://doi.org/10.1029/2005JB003766

Pollard, D., & DeConto, R. (2009). Modelling West Antarctic ice sheet growth and collapse through the past five million years. *Nature*, *458*, 329–332. https://doi.org/10.1038/nature07809

Rempel, A. W. (2008). A theory for ice-till interactions and sediment entrainment beneath glaciers. *Journal of Geophysical Research*, *113*(F1), F01013. https://doi.org/10.1029/2007JF000870

Rignot, E., Mouginot, J., & Scheuchl, B. (2016). *MEaSUREs Antarctic grounding line from differential satellite radar interferometry, version 2. NASA National Snow and Ice Data Center distributed active archive center*. https://doi.org/10.5067/IKBWW4RYHF1Q

Rignot, E., Mouginot, J., & Scheuchl, B. (2017). *MEaSUREs InSAR-based Antarctica ice velocity map, version 2. NASA National Snow and Ice Data Center distributed active archive center*. https://doi.org/10.5067/D7GK8F5J8M8R

Riverman, K. L., Anandakrishnan, S., Alley, R. B., Holschuh, N., Dow, C. F., Muto, A., et al. (2019). Wet subglacial bedforms of the NE Greenland Ice Stream shear margins. *Annals of Glaciology*, *60*(80), 1–9. https://doi.org/10.1017/aog.2019.43

Rooney, S. T., Blankenship, D. D., Alley, R. B., & Bentley, C. R. (1987). Till beneath ice stream B. 2. Structure and continuity. *Journal of Geophysical Research*, *92B*, 8913–8920. https://doi.org/10.1029/JB092iB09p08913

Scambos, T., Bell, R. E., Alley, R. B., Anandakrishnan, S., Bromwich, D. H., Brunt, K., et al. (2017). How much, how fast?: A review and science plan for research on the instability of Antarctica's Thwaites Glacier in the 21st century. *Global and Planetary Change*, *153*, 16–34. https://doi.org/10.1016/j.gloplacha.2017.04.008

Scherer, R. P., Aldahan, A., Tulaczyk, S., Possnert, G., Engelhardt, H., & Kamb, B. (1998). Pleistocene collapse of the West Antarctic ice sheet. *Science*, *281*, 82–85. https://doi.org/10.1126/science.281.5373.82

Schoof, C. (2005). The effect of cavitation on glacier sliding. *Proceedings of the Royal Society of London, Series A*, *461*, 609–627. https://doi.org/10.1098/rspa.2004.1350

Sergienko, O. V. (2012). The effects of transverse bed topography variations in ice-flow models. *Journal of Geophysical Research*, *117*, F03011. https://doi.org/10.1029/2011JF002203

Sergienko, O. V. (2013). Glaciological twins: Basally controlled subglacial and supraglacial lakes. *Journal of Glaciology*, *59*(213). https://doi.org/10.3189/2013JoG12J040

Sergienko, O. V., & Hindmarsh, R. C. A. (2013). Regular patterns in frictional resistance of ice-stream beds seen by surface data inversion. *Science*, *342*(6162), 1086–1089. https://doi.org/10.1126/science.1243903

Smith, A. M., Murray, T., Nicholls, K. W., Makinson, K., Aðalgeirsdóttir, G., Behar, A. E., & Vaughan, D. G. (2007). Rapid erosion, drumlin formation, and changing hydrology beneath an Antarctic ice stream. *Geology*, *35*(2), 127–130. https://doi.org/10.1130/G23036A.1

Smith, B. E., Gourmelen, N., Huth, A., & Joughin, I. (2017). Connected subglacial lake drainage beneath Thwaites Glacier, West Antarctica. *The Cryosphere*, *11*, 451–467. https://doi.org/10.5194/tc-11-451-2017

Spagnolo, M., Clark, C. D., Ely, J. C., Stokes, C. R., Anderson, J. B., Andreassen, K., et al. (2014). Size, shape and spatial arrangement of mega-scale glacial lineations from a large and diverse dataset. *Earth Surface Processes and Landforms*, *39*, 1432–1448. https://doi.org/10.1002/esp.3532

Stokes, G. G. (1851). On the effect of internal friction of fluids on the motion of pendulums. *Transactions of the Cambridge Philosophical Society*, *9*, 8–106. https://doi.org/10.1017/CBO9780511702266.002

Sun, S., Pattyn, F., Simon, E. G., Albrecht, T., Cornford, S., Calov, R., et al. (2020). Antarctic ice sheet response to sudden and sustained ice-shelf collapse (ABUMIP). *Journal of Glaciology*, 1–14. https://doi.org/10.1017/jog.2020.6710.1017/jog.2020.67

Walder, J. S. (1986). Hydraulics of subglacial cavities. *Journal of Glaciology*, *32*(112), 439–445. https://doi.org/10.3189/S0022143000012156

Walder, J. S., & Fowler, A. (1994). Channelized subglacial drainage over a deformable bed. *Journal of Glaciology*, *40*(134), 3–15. https://doi.org/10.3189/S0022143000003750

Weertman, J. (1957). On the sliding of glaciers. *Journal of Glaciology*, *3*(21), 33–38. https://doi.org/10.3189/S0022143000024709

Weertman, J. (1972). General theory of water flow at the base of a glacier or ice sheet. *Reviews of Geophysics and Space Physics*, *10*(1), 287–333. https://doi.org/10.1029/RG010i001p00287

Wellner, J. S., Heroy, D. C., & Anderson, J. B. (2006). The death mask of the Antarctic ice sheet: Comparison of glacial geomorphic features across the continental shelf. *Geomorphology*, *75*(1–2), 157–171. https://doi.org/10.1016/j.geomorph.2005.05.015

Whillans, I. M. (1976). Radio-echo layers and the recent stability of the West Antarctic ice sheet. *Nature*, *264*, 152–155. https://doi.org/10.1038/264152a0

Whillans, I. M., & Johnsen, S. J. (1983). Longitudinal variations in glacial flow: Theory and test using data from the Byrd Station Strain Network, Antarctica. *Journal of Glaciology*, *29*(101), 78–97. https://doi.org/10.3189/S0022143000005165

Whittecar, G. R., & Mickelson, D. M. (1977). Sequence of till deposition and erosion in drumlins. *Boreas*, *6*, 213–217. https://doi.org/10.1111/j.1502-3885.1977.tb00350.x

Winberry, J. P., & Anandakrishnan, S. (2004). Crustal structure of the West Antarctic rift system and Marie Byrd Land hotspot. *Geology*, *32*(11), 977–980. https://doi.org/10.1130/G20768.1

Wolovick, M. J., Creyts, T. T., Buck, W. R., & Bell, R. E. (2014). Traveling slippery patches produce thickness-scale folds in ice sheets. *Geophysical Research Letters*, *41*, 8895–8901. https://doi.org/10.1002/2014GL062248

Woodard, J. B., Zoet, L. K., Benediktsson, Í. Ö., Iverson, N. R., & Finlayson, A. (2020). Insights into drumlin development from ground-penetrating radar at Múlajökull, Iceland, a surge-type glacier. *Journal of Glaciology*, *66*(259), 822–830. https://doi.org/10.1017/jog.2020.50

Zoet, L. K., & Iverson, N. R. (2020). A slip law for glaciers on deformable beds. *Science*, *368*(6486), 76–78. https://doi.org/10.1126/science.aaz1183

Zoet, L. K., Rawling, J. E., Woodard, J. B., Barrette, N., & Mickelson, D. M. (2021). Factors that contribute to the elongation of drumlins beneath the Green Bay Lobe, Laurentide Ice Sheet. *Earth Surface Processes and Landforms*, *1*, 2540–2550. https://doi.org/10.1002/esp.5192

References From the Supporting Information

Alley, R. B. (2000). Continuity comes first: Recent progress in understanding subglacial deformation. In A. J. Maltman, & M. J. Hambrey (Eds.), *Deformation of glacial materials* (Vol. 176, pp. 171–179). Geological Society of London, Special Publication. https://doi.org/10.1144/GSL.SP.2000.176.01.13

Alley, R. B., Cuffey, K. M., Evenson, E. B., Strasser, J. C., Lawson, D. E., & Larson, G. J. (1997). How glaciers entrain and transport basal sediment: Physical constraints. *Quaternary Science Reviews*, *16*, 1017–1038. https://doi.org/10.1016/S0277-3791(97)00034-6

Atre, S. R., & Bentley, C. R. (1993). Laterally varying basal conditions beneath ice streams B and C: West Antarctica. *Journal of Glaciology*, *39*, 507–514. https://doi.org/10.3189/S0022143000016403

Bartholomew, I., Nienow, P., Mair, D., Hubbard, A., King, M. A., & Sole, A. (2010). Seasonal evolution of subglacial drainage and acceleration in a Greenland outlet glacier. *Nature Geoscience*, *3*, 408–411. https://doi.org/10.1038/ngeo863

Blankenship, D. D., Bentley, C. R., Rooney, S. T., & Alley, R. B. (1986). Seismic measurements reveal a saturated porous layer beneath an active Antarctic ice stream. *Nature*, *322*, 54–57. https://doi.org/10.1038/322054a0

Blankenship, D. D., Bentley, C. R., Rooney, S. T., & Alley, R. B. (1987). Till beneath ice stream B. 1. Properties derived from seismic travel times. *Journal of Geophysical Research*, *92B*, 8903–8912. https://doi.org/10.1029/JB092iB09p08903

Boulton, G. S., & Hindmarsh, R. C. A. (1987). Sediment deformation beneath glaciers: Rheology and geological consequences. *Journal of Geophysical Research*, *92*(B9), 9059–9082. https://doi.org/10.1029/JB092iB09p09059

Byers, J., Cohen, D., & Iverson, N. R. (2012). Subglacial clast/bed contact forces. *Journal of Glaciology*, *58*(207), 89–98. https://doi.org/10.3189/2012JoG11J126

Christoffersen, P., Bougamont, M., Carter, S. P., Fricker, H. A., & Tulaczyk, S. (2014). Significant groundwater contribution to Antarctic ice streams hydrologic budget. *Geophysical Research Letters*, *41*, 2003–2010. https://doi.org/10.1002/2014gl059250

Dow, C. F., Kulessa, B., Rutt, I. C., Tsai, V. C., Pimentel, S., Doyle, S. H., et al. (2015). Modeling of subglacial hydrological development following rapid supraglacial lake drainage. *Journal of Geophysical Research: Earth Surface*, *120*, 1127–1147. https://doi.org/10.1002/2014JF003333

Dreimanis, A. (1989). Tills: Their genetic terminology and classification. In R. P. Goldthwait, & C. L. Matsch (Eds.), *Genetic classification of glacigenic deposits* (pp. 17–83). A. A. Balkema.

Engelhardt, H., & Kamb, B. (1998). Basal sliding of ice stream B, West Antarctica. *Journal of Glaciology*, *44*(147), 223–230. https://doi.org/10.3189/S0022143000002562

Fischer, U. H., & Clarke, G. K. C. (2001). Review of subglacial hydro-mechanical coupling: Trapridge Glacier, Yukon Territory, Canada. *Quaternary International*, *86*(1), 29–43. https://doi.org/10.1016/S1040-6182(01)00049-0

Flowers, G. E. (2015). Modelling water flow under glaciers and ice sheets. *Proceedings of the Royal Society of London, Series A*, *471*. https://doi.org/10.1098/rspa.2014.0907

Hallet, B. (1979). A theoretical model of glacial abrasion. *Journal of Glaciology*, *23*(89), 39–50. https://doi.org/10.3189/S0022143000029725

Hallet, B. (1996). Glacial quarrying: A simple theoretical model. *Annals of Glaciology*, *22*, 1–8. https://doi.org/10.3189/1996AoG22-1-1-8

Hansen, D. D., & Zoet, L. K. (2019). Experimental constraints on subglacial rock friction. *Annals of Glaciology*, *60*(80), 37–48. https://doi.org/10.1017/aog.2019.47

Iverson, N. R. (1990). Laboratory simulations of glacial abrasion: Comparison with theory. *Journal of Glaciology*, *36*(124), 304–314. https://doi.org/10.3189/002214390793701264

Iverson, N. R., Baker, R. W., Hooke, R. L., Hanson, B., & Jansson, P. (1999). Coupling between a glacier and a soft bed: I. A relation between effective pressure and local shear stress determined from till elasticity. *Journal of Glaciology*, *45*(149), 31–40. https://doi.org/10.3189/S0022143000003014

Iverson, N. R., Hanson, B., Hooke, R. L., & Jansson, P. (1995). Flow mechanism of glaciers on soft beds. *Science*, *267*(5194), 80–81. https://doi.org/10.1126/science.267.5194.80

Kavanaugh, J. L., & Clarke, G. K. C. (2006). Discrimination of the flow law for subglacial sediment using in situ measurements and an interpretation model. *Journal of Geophysical Research*, *111*(F1), F01002. https://doi.org/10.1029/2005JF000346

Kulessa, B., Hubbard, A. L., Booth, A. D., Bougamont, M., Dow, C. F., Doyle, S. H., et al. (2017). Seismic evidence for complex sedimentary control of Greenland Ice Sheet flow. *Science Advances*, *3*, e1603071. https://doi.org/10.1126/sciadv.1603071

Peters, L. E., Anandakrishnan, S., Alley, R. B., & Smith, A. M. (2007). Extensive storage of basal meltwater in the onset region of a major West Antarctic ice stream. *Geology*, *35*(3), 251–254. https://doi.org/10.1130/G23222A.1

Rempel, A. W., & Meyer, C. R. (2019). Premelting increases the rate of regelation by an order of magnitude. *Annals of Glaciology*, *65*(251), 518–521. https://doi.org/10.1017/jog.2019.33

Röthlisberger, H. (1968). *Erosive processes which are likely to accentuate or reduce the bottom relief of valley glaciers* (Vol. 79, pp. 87–97). IASH Publ.(General Assembly of Bern 1967 –Snow and Ice).

Siegert, M. J., Carter, S., Tabacco, I., Popov, S., & Blankenship, D. D. (2005). A revised inventory of Antarctic subglacial lakes. *Antarctic Science*, *17*(3), 453–460. https://doi.org/10.1017/S0954102005002889

Schmidt, B. E., Washam, P., Davis, P. E. D., Nicholls, K., Lawrence, J., Smith, J., et al. (2020). *Melting at the grounding zone of Thwaites glacier observed by icefin. C057-04*. American Geophysical Union Fall Meeting. Retrieved from https://agu.confex.com/agu/fm20/meetingapp.cgi/Paper/735407

Schroeder, D. M., Blankenship, D. D., & Young, D. A. (2013). Water system transition beneath Thwaites Glacier. *Proceedings of the National Academy of Sciences*, *110*(30), 12225–12228. https://doi.org/10.1073/pnas.1302828110

Shen, W., Wiens, D., Lloyd, A., & Nyblade, A. (2020). A geothermal heat flux map of Antarctica empirically constrained by seismic structure. *Geophysical Research Letters*, *47*, e2020GL086955. https://doi.org/10.1029/2020gl086955

Tulaczyk, S., Kamb, B., & Engelhardt, H. (2008). Estimates of effective stress beneath a modern West Antarctic ice stream from till pre-consolidation and void ratio. *Boreas*, *30*, 1010–1114. https://doi.org/10.1111/j/1502-3885.2001.tb01216.x

Walder, J. (2010). Röthlisberger channel theory: Its origins and consequences. *Journal of Glaciology*, *56*(200), 1079–1086. https://doi.org/10.3189/002214311796406031

Walder, J. S. (1982). Stability of sheetflow of water beneath temperateglaciers and implications for glacier surging. *Journal of Glaciology*, *28*(99), 273–293. https://doi.org/10.3189/S0022143000011631

Zoet, L. K., Alley, R. B., Anandakrishnan, S., & Christianson, K. (2013). Accelerated subglacial erosion in response to stick-slip motion. *Geology*, *41*(2), 159–162. https://doi.org/10.1130/G33624.1

Journal of Geophysical Research—Earth Surface

Supporting Information for

Bedforms of Thwaites Glacier, West Antarctica: Character and Origin

R.B. Alley[1], N. Holschuh[2,3], D.R. MacAyeal[4], B.R. Parizek[1], L. Zoet[5], K. Riverman[6,7], A. Muto[8], K. Christianson[2], E. Clyne[1], S. Anandakrishnan[1], N. Stevens[5], GHOST Collaboration[†]

[1]Department of Geosciences, and Earth and Environmental Systems Institute, Pennsylvania State University, University Park, PA, USA

[2]Department of Earth and Space Sciences, University of Washington, Seattle, WA, USA

[3]Department of Geology, Amherst College, Amherst, MA, USA

[4]Department of Geophysical Sciences, University of Chicago, Chicago, IL, USA

[5]Department of Geoscience, University of Wisconsin, Madison, WI, USA

[6]College of Earth, Ocean, and Atmospheric Sciences, Oregon State University, Corvallis, OR, USA

[7]Departmen of Environmental Studies, University of Portland, Portland, OR, USA

[8]Department of Earth and Environmental Science, Temple University, Philadelphia, PA, USA

[†]https://thwaitesglacier.org/projects/ghost

Corresponding author: Richard B. Alley (rba6@psu.edu)

Contents of this file

Introduction

The numerical simulations featured in Figures 4 and 5 were designed as thought experiments with simplified dynamics, parameters and geometries so as to illustrate the ideas discussed in the manuscript. Here we describe how the simulations were formulated, document software used, list parameter values and note the location where numerical data and software (COMSOL model files) are archived for use by readers of the manuscript.

S1 Model description

COMSOL 5.5, a commercially maintained and distributed finite-element software package, augmented by the Computational Fluid Dynamics (CFD) and Heat Transfer modules, was used to perform all numerical simulations. A multi-part 2-d numerical domain was developed using the geometry primitive shapes provided in the COMSOL geometry interface. For numerical simulations related to Fig. 4, the domain consisted of an ice layer and a bed layer with a circular bump in the bed of radius 100 m. For simulations related to Fig. 5, a 'moat' was added to the ice layer by incising a depression of circular, wedge shaped or elliptical geometry into the bed layer at the leading edge of the hemispherical bump in the bed layer.

Viscous flow, with a viscosity of 10^{13} Pa s, was simulated in the ice layer using boundary conditions specified in Fig. 4a, as well as for additional ice-bed boundary conditions that were separately tested to estimate robustness of results shown in Fig. 4. This simulation was conducted using the COMSOL Fluid Flow: Single Phase Flow: Laminar Flow module with inertial terms neglected. Basal boundary conditions at the ice/bed interface were experimented with to assess robustness of results, and were specified as either free-slip everywhere, no-slip everywhere or free-slip on horizontal planes and no-slip on the bump. Ice density was specified as 900 kg m^{-3}. The boundary condition on the top of the ice layer (dimensions are shown in Fig. 4) was an applied shear stress, parallel to the flat parts of the ice/bed interface, equal to 100 kPa. The upstream and downstream boundaries of the ice layer were assumed to be periodic with a zero pressure difference. Gravity and hydrostatic pressure in the simulation were neglected, hence all results are relative to a zero pressure reference level.

Heat transfer in the ice and bed layers was simulated using the Heat Transfer in Solids module of COMSOL, which implements conduction only. (Experiments with advection terms active in the ice layer were conducted, but not used in the research presented here.) Thermal parameters for the ice and rock were: density, 900 and 2750 kg m^{-3}, respectively; thermal conductivity, 2 and 2 W m^{-1} K^{-1}, respectively; heat capacity, 2100 and 800 J K^{-1}, respectively. The thermal boundary condition applied at the ice/bed interface was that temperature was equal to the pressure melting temperature T_m given by, $T_m = 273.15 - P\,C$, where P is the pressure on the ice/bed interface evaluated from the viscous flow solution described above, and $C = 0.74 \times 10^{-7}$ K Pa^{-1}. Evaluation of net heat flux into the ice/bed interface was done by summing the outward normal conductive heat flux emerging from the ice and bed layers. Boundary conditions on the top of the ice

layer and bottom of the rock layer were T=273.15 K and no normal heat flux, respectively. Periodic boundary conditions at the upstream and downstream sides of the ice and rock layers were specified with a zero temperature difference.

The finite-element mesh was specified to be 'physics-controlled' and 'extremely fine' in the mesh parameter module of COMSOL for all simulations.

To assess robustness of conclusions drawn from the numerical simulations, particularly for those represented in Fig. 4, we conducted experiments with 3 different boundary condition formulations applied to the ice/bed interface: free-slip everywhere, no-slip everywhere, and no-slip on the bump, free-slip on the horizontal surfaces. Figure S1 presents a comparison of these three sensitivity tests.

S2 Experiments with moats

Numerical simulations were conducted to examine the effects of an eroded 50 m deep moat-like bedform in the immediate upstream area of the bed bump shown in Fig. 4. The geometry of these simulations is shown in Fig. S2. For the results shown in Fig. 5, a free-slip boundary condition was applied to all parts of the ice/bed interface except that a no-slip condition was applied on the surface of the bump immediately downstream of the moat. To assess robustness of the idealized numerically facilitated thought experiments, we present in Fig. S3 a comparison of the results of Fig. 5 with two additional simulations, one where the ice/bed boundary condition was free slip everywhere and the other where the ice/bed boundary condition was no slip everywhere. We additionally assessed the effect of upstream length of the moat geometry, by replacing the semicircular moat with an elliptical moat with variable semi-major axis length (Fig. S4).

In general, the experiments conducted with moat geometries of all types suffered from the well-known singularity of pressure and temperature that exist on the upstream corner of the moat, where it joins with the flat bed upstream of the moat and bump. This singularity is described in Barcilon and MacAyeal (1993) and MacAyeal (2019), and exists on 'external corners' where the ice must deform with infinite strain rate to round the corner where a free-slip condition is applied. Clearly, the idealized physics of the numerical experiments is inadequate for dealing with such singularities, as there is no cavitation or other effects incorporated here. We recommend that the results of the moat experiments be interpreted in the most idealized manner with awareness that further study is needed, with more robust, physically complex models, to examine the dynamics of an eroding moat in greater detail.

S3 Model software and data archival

The COMSOL models used for Figs. 4 and 5, and model-output data, are archived for public availability according to the description provided in the main manuscript, at http://www.datacommons.psu.edu/commonswizard/MetadataDisplay.aspx?Dataset=6181 with doi https://doi.org/10.26208/ce9f-sm73 . The model-output data are chosen to provide a means to repeat the model calculations with numerical simulation software that is open-access (COMSOL is a commercially distributed finite-element package).

S4 Effects of ice flow against obstacles on basal behavior in survey region

S4a Water flow and effective pressure

Strong evidence summarized below indicates that the water system over the soft till regions in our survey grids of Thwaites Glacier is dominantly distributed rather than channelized, and generally at pressure very close to the ice-overburden pressure. In such a system, the large stoss-side increase in ice-bed contact pressure caused by ice flow against bedrock obstacles will divert subglacial water flow, coupling the ice more strongly to any subglacial till to increase the deformational flux, and thus removing till to allow bedrock erosion.

The most direct information on the basal water system of Thwaites Glacier in our study region comes from physical interpretation of seismic surveys demonstrating that the bed has very low acoustic impedance in large basins and in lee-side positions (Muto et al., 2019a; 2019b; Clyne et al., 2020). Such low acoustic impedances indicate unconsolidated, high-porosity, soft water-saturated sediment that likely is deforming, and require that the water pressure supports almost the entire overburden pressure (e.g., Blankenship et al., 1986; Atre and Bentley, 1993; Muto et al., 2019a). Observations from other sites show distributed rather than channelized water systems associated with such till; water would drain away through groundwater flow in the absence of distributed resupply at the base of the ice (e.g., Kamb, 2001; see below). The low acoustic impedance also shows that the till is not suffering net loss of water by freeze-on to the ice as beneath the Siple Coast ice streams (Christoffersen et al., 2014), consistent with net melting beneath the ice of Thwaites Glacier (e.g., Hoffman et al., 2020).

Subglacial water pressure, P_w, is often expressed through the effective pressure $N=P-P_w$, with P the ice-overburden pressure. The observed low acoustic impedances in lee-side positions and extensive basins beneath Thwaites Glacier indicate that N is small there ($<10^5$ Pa or $<<10^5$ Pa). Tills with similarly low acoustic impedances have been widely observed beneath ice streams on the Siple Coast of West Antarctica, where Tulaczyk et al. (2008) found that $N<2.5\times10^4$ Pa, and perhaps as low as $N=2\times10^3\pm0.8\times10^3$ Pa (also see Blankenship et al., 1986; 1987; Peters et al., 2007) in association with widespread, high-pressure, distributed water including subglacial lakes (e.g., Kamb, 2001). Subglacial lakes have been detected beneath Thwaites Glacier (Smith et al., 2017; Hoffman et al., 2020) and in other settings beneath the Antarctic ice sheet including upglacier of Thwaites in central West Antarctica (Siegert et al., 2005), indicating N=0 in those places.

The small effective pressures over the soft tills beneath Thwaites indicate a distributed water system, lacking well-developed, steady Röthlisberger (R) (Röthlisberger, 1968) channels capable of rapidly transmitting large quantities of water and sediment. This lack of sustained, influential R-channels is not surprising. The bed of Thwaites in our study area is supplied only by basal meltwater with no moulin drainages from the surface, and basal meltwater on mountain glaciers and in coastal regions of the Greenland ice sheet is unable to maintain the vigorous surface-melt-fed summertime R-channel system through even a few winter months (Cuffey and Paterson, 2010; also see Bartholomew et al., 2010; Dow et al., 2015; Kulessa et al., 2017; note that the proposed Schroeder et al., 2013 transition beneath Thwaites is near the downglacier end of our downglacier survey block). As argued by Walder (1982; 2010), ice flow pinches off small or incipient R-channels by carrying them against bumps in the bed, requiring large water fluxes to maintain open channels. This problem of flow against bumps is reduced in regions of soft tills, but interactions with till there favor a distributed system (Walder and Fowler, 1994; Kamb, 2001). In a distributed water system, whether films, linked cavities, or canals, the water pressure, storage, typical thickness and lateral extent all increase with supply (e.g., Walder and Fowler, 1994; Alley, 1996; Cuffey and Paterson, 2010; Flowers, 2015).

Muto et al. (2019b and Holschuh et al., 2020) calculated the gradient in the hydrological potential for the distributed water system indicated by seismic and radar data, assuming a spatially and temporally constant effective pressure. Averaged over the upglacier grid of Figure 1, they found an along-ice-flow gradient of ~15 Pa/m, with important variations including local reversals over shorter distances, and with a gradient of generally much smaller magnitude over the till-lubricated regions. Thus, ice-pressure perturbations of order 10^5 Pa caused by ice flow against major bumps are large compared to variations over similar length scales caused by ice and bed geometry alone, and compared to any N that is expected nearby. Such perturbations thus will have major effects on meltwater routing, tending to divert water from upglacier sides of obstacles, over a considerable distance that scales with the obstacle size as discussed above (Holschuh et al., 2020), and in section 4 of the paper.

S4b Controls on till flux

Water diversion from upglacier sides of obstacles will couple ice more strongly to till and increase till flux by deformation, with lee-side decoupling leading to deposition there. The divergence of this deforming-bed till flux is the most important factor in erosion and deposition generating bedforms, as discussed next.

Data across a wide range of subglacial conditions show that soft tills deform (reviewed by Alley, 2000). The somewhat limited available data indicate that till flux by subglacial deformation exhibits a maximum at some intermediate effective pressure N. Deformation is believed to be suppressed, giving lodgement till, at very low water

pressure/high N in sufficiently compacted till (e.g., Boulton and Hindmarsh, 1987; Driemanis, 1989); thus, there are circumstances in which adding water and thus decreasing N can increase till deformation. Deformation is also suppressed at high water pressure/low N as water decouples ice from the bed, as discussed next. Well-validated quantitative relations between till flux and N for a range of conditions are generally not known, but the available evidence summarized below indicates that adding water and thus decreasing N for the soft tills of Thwaites will decrease deformational till flux (also see Muto et al., 2019b).

For Antarctica, the best data sets on subglacial tills are from the Siple Coast. The extensive borehole experiments by Engelhardt and Kamb (1998) and Kamb (2001) documented deforming till, with the measured deformation primarily concentrated in a thin layer just below the ice (~3-25 cm thick). Adding water from the boreholes decoupled ice from the bed and decreased the till deformation.

Observations in soft-bedded regions of Storglaciären, Sweden (Iverson et al., 1995) and Trapridge Glacier, Canada (Fischer and Clarke, 2001; Kavanaugh and Clarke, 2006) similarly found that, in response to rising water pressure leading to reduction in N, deformation decreased in deforming subglacial tills. In some cases, adding water caused till deformation to temporarily reverse sign, as the ice was decoupled from the bed and the till responded elastically to the reduced stress from the ice (Iverson et al., 1995; 1999). As noted by Muto et al. (2019b), time-variation in surface-water input drove the fluctuations at Trapridge Glacier and Storglaciären, a process that does not happen beneath Thwaites (lake drainages may locally cause perturbations; Smith et al. 2017; Hoffman et al, 2020). Nonetheless, physical similarity suggests that greater water supply or smaller hydrologic-potential gradient will tend to decrease N and thus decrease till flux by deformation beneath Thwaites, as also described in Muto et al. (2019b).

The tendency for ice to regelate into till when N is high (e.g., Meyer et al., 2018) does favor sediment flux into the ice as well as subglacial till deformation. The basal ice likely contains some debris, based on analogy to many other sites, and based on the images from the 2019-2020 field season from beneath the ice shelf of Thwaites Glacier showing debris-bearing basal ice (Schmidt et al., 2020). As argued by Muto et al. (2019b), though, the divergence of this debris flux in ice is unlikely to be large compared to the divergence in deforming beds. Regelation into subglacial till will be slow, in part because the generally fine-grained nature of tills slows or stops regelation (e.g., Alley et al., 1997, section 4.2), and because the regional high geothermal flux (e.g., Shen et al., 2020) and heat of sliding act to oppose regelation into the bed. Changes along ice flow in debris flux carried within ice thus will be small, leaving divergence in deforming-till flux to balance deposition and erosion.

S4c Abrasion and plucking

Our main interest here is in the large-scale features of the bed of Thwaites Glacier. We note, though, that pressure is raised upglacier of any obstacle to flow. This includes small bumps, and should also include small abrading clasts in the ice for which regelation

dominates the relative motion. The Weertman solution for regelation around obstacles emphasized the heat flow through the obstacle to the stoss-side face. As shown by Figure 5 of MacAyeal (2019), however, and in Figure 4 here, a numerical model for that heat flow routes a significant fraction from the low-pressure region on the lee-side bed to the high-pressure region on the stoss-side bed extending well beyond the obstacle itself; in the Weertman model, this would cause melting upglacier of the clast on the horizontal bed and freezing downglacier.

If the obstacle were an abrading clast that did not generate a lee-side cavity, the stoss-side melting and lee-side freezing on the bed would tend to cause lee-side upward motion of the ice and stoss-side downward motion, producing a torque on the clast opposing the tendency for the clast to rotate rather than abrade, and thus favoring faster abrasion (Hallet, 1979; Iverson, 1990; Byers et al., 2012). Perhaps more importantly, if the clast develops a lee-side cavity (e.g., Hansen and Zoet, 2019), the stoss-side melting would not be balanced by lee-side freeze-on along the bed, giving a net downward motion of the ice in contact with the clast that could be much more rapid than usually calculated in the Hallet (1979) abrasion model. This in turn would give a greater normal stress of the clast on the bed than in that solution. This may help explain why measured clast-bed contact forces are so high (Byers et al., 2012). A full analysis of these and related issues, including the role of premelting (Rempel and Meyer, 2019), is beyond the scope of this manuscript, but may be of considerable interest. Note further that a large obstacle (e.g., the 100-m scale in Figure 6) that raises the basal pressure over a large stoss-side area will have a small but widespread effect on abrasion by lowering the melting point for ice as it flows into that region, hence slightly increasing the basal melt rate and thus the convergence rate of ice with the bed around any abrading clasts.

Plucking is favored by high contact forces between ice and bed (Hallet, 1996), up to and including generation of stick-slip behavior (e.g., Zoet et al., 2013). Thus, higher drag from abrading clasts can increase erosion from plucking as well, in those regions where debris-laden ice contacts bedrock, contributing to moat erosion as discussed below.

S5 Additional References Cited in Supporting Information

Barcilon, V., & MacAyeal, D. R. (1993). Steady flow of a viscous ice stream across a no-slip/free-slip transition at the bed. *Journal of Glaciology*, 39, 167-185. https://doi.org/10.3189/S0022143000015811

MacAyeal, D.R. (2019). Revisiting Weertman′s tombstone bed. *Annals of Glaciology*, *60*(80), 1–9. https://doi.org/10.1017/aog.2019.31

Supplemental Figures

Figure S1 Comparison of ice/bed boundary condition specification effects on temperature and net heat flux to the ice/bed interface (A - C, free-slip everywhere, free-slip on horizontal surfaces/no-slip on bump, no-slip everywhere, respectively; D, comparison of net heat flux in mW to the ice/bed interface). Line along the ice/bed interface in A - C is colored red where there is net heat convergence (melting) and blue where there is net heat divergence (freezing). Streamlines show heat flux (arrow size and line density not significant). S1-C shows the same conditions as Figure 4.

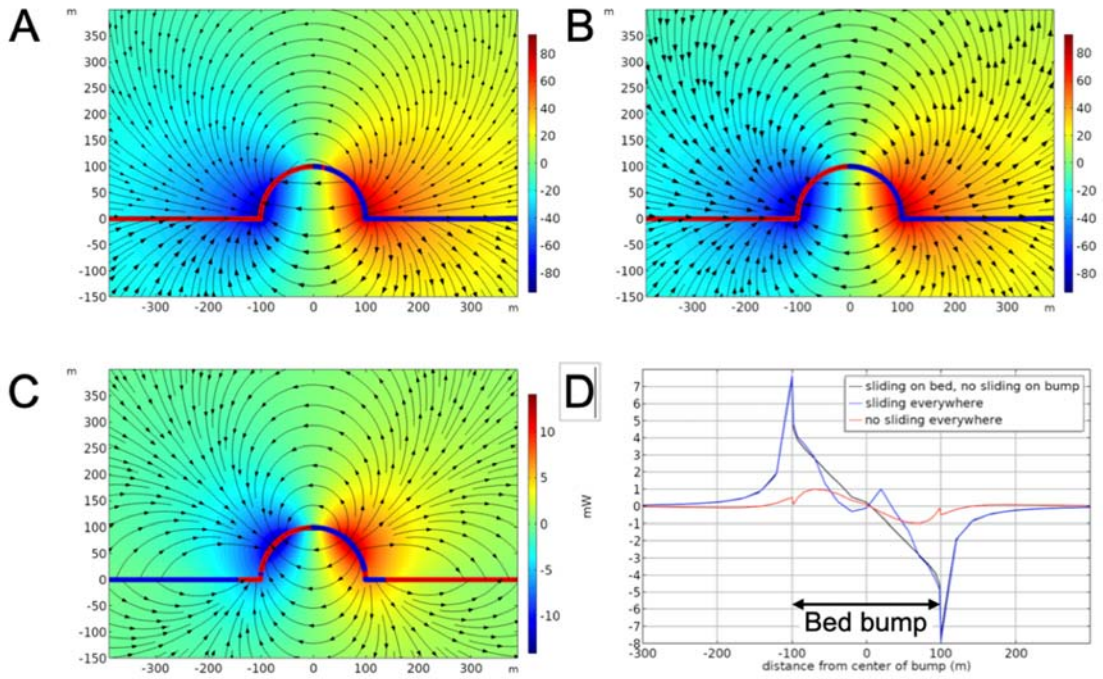

Figure S2 Geometry of the numerical experiments involving a moat in the immediate foreground of the bump on the bed. The depth of the moat in all simulations is 50 m, which is half of the height of the bump. Experiments were conducted where the upstream extent of the moat was enlarged (Fig. S4) by changing the moat from a semicircular cross section to one with an elliptical cross section.

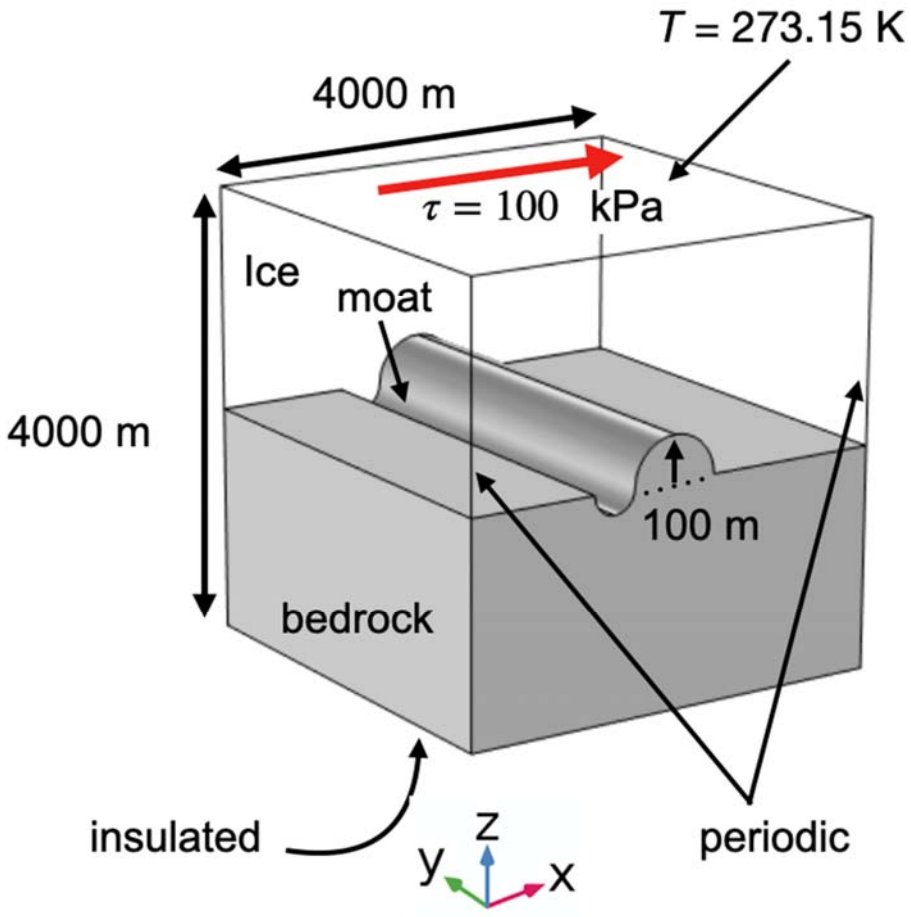

Figure S3 Comparison of ice/bed boundary condition specification effects on temperature and net heat flux to the ice/bed interface in the semicircular moat-geometry experiments (A - C, free-slip everywhere, free-slip on horizontal surfaces/no-slip on bump, no-slip everywhere, respectively; D, comparison of net heat flux in mW to the ice/bed interface). For reference, the radius of the bump is 100 m and the depth of the moat is 50 m. Line along the ice/bed interface in A - C is colored red where there is net heat convergence (melting) and blue where there is net heat divergence (freezing). Streamlines show heat flux (arrow size and line density not significant). S3-C shows the same conditions as Figure 5.

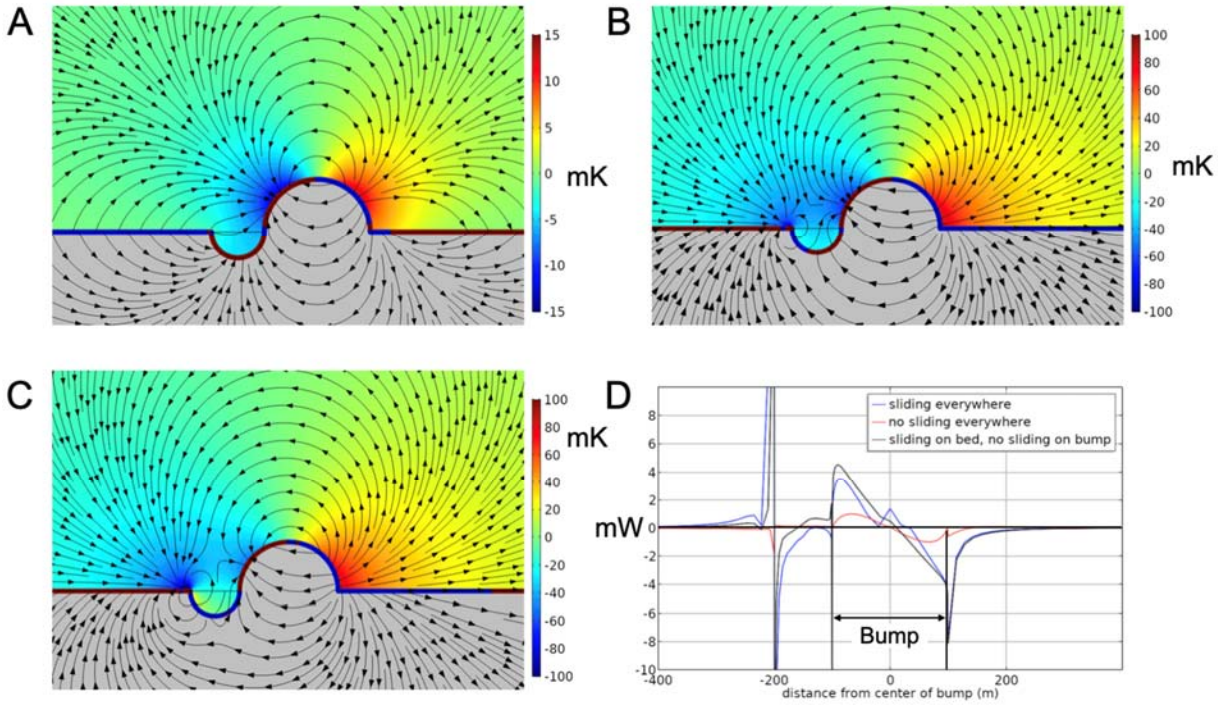

Figure S4 Comparison of differing upstream extent (300 m, 500 m, 900 m, panels A - C, respectively) of semielliptical moat geometry for an ice/bed boundary condition that is free slip everywhere except no-slip on the semicircular boundary of the bump. For reference, the radius of the bump is 100 m and the maximum depth of the moat is 50 m. Line along the ice/bed interface in A - C is colored red where there is net heat convergence (melting) and blue where there is net heat divergence (freezing). Streamlines show heat flux (arrow size and line density not significant).

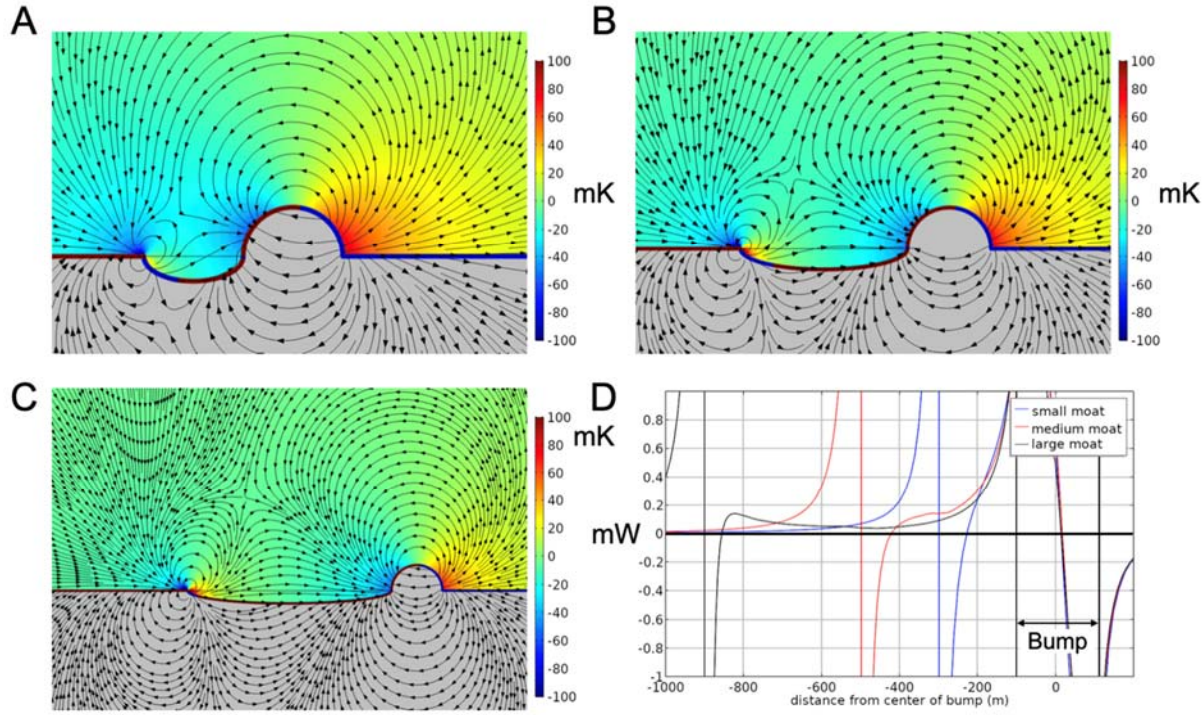

Appendix A

Members of the Geophysical Habitat of Subglacial Thwaites (GHOST) Collaboration team are Andy Smith, Rob Arthern, Robert Bingham, Alex Brisbourne, Olaf Eisen, Coen Hofstede, Bernd Kulessa, Leigh Sterns, Paul Winberry, Julien Bodart, Louise Borthwick, Elizabeth Case, Chloe Gustafson, Jonny Kingslake, Helen Ockenden, Charlotte Schoonman, and Emily Schwans.